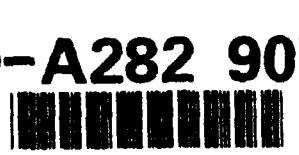

3.

231500-5-T

DATA FUSION INTERIM REPORT

R. Shuchman
C. Russel
C. Wackerman

Center for Earth Sciences

June 1991

Prepared for:
Office of Naval Research
Charles Luther, Scientific Officer
800 N. Quincy
Arlington, VA 22217-5000

Contract No.: N00014-90-C-0148

ERIM P.O. Box 134001
Ann Arbor, MI 48113-4001

REPORT DOCUMENTATION PAGE

Form Approved
OMB No. 0704-0188

1. AGENCY USE ONLY (Leave blank)	2. REPORT DATE	3. REPORT TYPE AND DATES COVERED
	June 1991	Technical 5/1/90 - 4/30/91

4. TITLE AND SUBTITLE

DATA FUSION INTERIM REPORT

5. FUNDING NUMBERS

N00014-90-C-0148

6. AUTHOR(S)

R. Shuchman C. Wackerman
C. Russel

7. PERFORMING ORGANIZATION NAME(S) AND ADDRESS(ES)

Environmental Research Institute of Michigan
P.O. Box 134001
Ann Arbor, MI 48113-4001

8. PERFORMING ORGANIZATION REPORT NUMBER

231500-5-T

9. SPONSORING/MONITORING AGENCY NAME(S) AND ADDRESS(ES)

Office of Naval Research
800 N. Quincy
Arlington, VA 22217-5000

10. SPONSORING/MONITORING AGENCY REPORT NUMBER

11. SUPPLEMENTARY NOTES

12a. DISTRIBUTION/AVAILABILITY STATEMENT

Unlimited

12b. DISTRIBUTION CODE

13. ABSTRACT (Maximum 200 words)

For many years now a large amount of research has gone into developing algorithms for extracting arctic ice geophysical parameters from remote sensors. The Special Sensor Microwave Imager (SSM/I), the Advanced Very High Resolution Radiometer (AVHRR), and airborne and satellite synthetic aperture radar (SAR) systems are just some examples of sensors that can provide various geophysical products. With the problem well in hand of what a single sensor can provide about the arctic regions, the next step is to understand how combining sensors can increase our geophysical information. Such combining, or "fusing", of sensor information has the potential for tremendous payoffs since individual sensors have different advantages and disadvantages and their fusion would, in theory,be able to utilize the strengths of each while overcoming their weaknesses. This paper provides the initial foundation for additional data fusion studies.

14. SUBJECT TERMS	15. NUMBER OF PAGES
Special Sensor Microwave Imager (SSM/I) Advanced Very High Resoultion Radiometer (AVHRR) Synthetic Apeture Radar (SAR)	69
	16. PRICE CODE

17. SECURITY CLASSIFICATION OF REPORT	18. SECURITY CLASSIFICATION OF THIS PAGE	19. SECURITY CLASSIFICATION OF ABSTRACT	20. LIMITATION OF ABSTRACT
Unclassified	Unclassified	Unclassified	

TABLE OF CONTENTS

FIGURES

FIGURES (cont.)

FIGURES (concluded)

TABLES

1.0 INTRODUCTION AND RESEARCH SUMMARY

For many years now a large amount of research has gone into developing algorithms for extracting arctic ice geophysical parameters from remote sensors. Multiyear ice concentrations, total ice concentrations, wind speeds and ice edge locations from the Special Sensor Microwave Imager (SSM/I), sea surface temperatures, ice edge and ice kinematics from the Advanced Very High Resolution Radiometer (AVHRR), ice concentrations, ice types, ice kinematics, floe statistics and ridge characteristics from airborne and satellite synthetic aperture radar (SAR) systems are just some examples of the work that has been performed. Many of these products are now routinely used by researchers and by centers such as the Joint Ice Center (JIC) that produce weekly ice information maps. With the problem well in hand of what a single sensor can provide about the arctic regions, the next step is to understand how combining sensors can increase our geophysical information. Such combining, or "fusing", of sensor information has the potential for tremendous payoffs since individual sensors have different advantages and disadvantages and their fusion would,in theory,be able to utilize the strengths of each while overcoming their weaknesses.

Data fusion investigations can be broken down into three main categories. The first category, and the one pursued by a number of researchers, is the use of data fusion for algorithm verification. That is, using the geophysical products that are derived from one sensor to "truth" the geophysical products from another sensor. If the products from the first sensor have been proved correct, then this will verify the products from the second sensor. What is more usual, deriving that the two sensors give similar results increases the confidence that the results are accurate, even if it does not directly prove it.

After establishing a confidence that the individual sensors are generating accurate sea ice products, the second category of data fusion is to combine the geophysical products from each sensor to generate a more comprehensive picture of a scene. Ice edge and concentration from one sensor, ice floe statistics from a different, wind speed from a third, and temperature from a fourth can all be combined into a uniform data set (i.e., the same spatial and temporal grid) to give a global view of the environment of the scene. This can greatly improve the understanding of experimental data that may depend on a number of environmental parameters. For example, understanding the propagation of acoustic waves depends in part on the ice ridge statistics and water temperature; geophysical parameters that can be provided using data fusion techniques.

The final category of data fusion investigations is where the real payoff could lie; combining the raw measurements made by the individual sensors to generate geophysical information that any sensor alone could not generate. This is the newest, and hardest, aspect of data fusion and involves an analysis of combined sensor data on par with the analysis of individual sensor measurements that has been actively pursued the last two decades. It is the purpose of this and future studies to determine if such payoffs are even possible and how to achieve them.

This study has been an initial start to the final data fusion goal; the generation of practical algorithms for deriving new geophysical information from data fusion. We are not at this goal, but we have laid down the foundation necessary to answer some very important questions about the utility of data fusion, and how to achieve it. Specifically, the results of this study are summarized below.

The first step in analyzing data fusion capability is to generate a registered data set of different sensors. That is, to map geophysical products from different sensors taken from approximately the same time onto the same spatial grid. This has been done for four data sets. The first two were taken from the Coordinated Eastern

Arctic Regional Experiment (CEAREX) and contain SAR, SSM/I and AVHRR data. The last two were taken from the Marginal Ice Zone Experiment (MIZEX) 1987 and the Alaska collection in 1988 and contain SAR and Geodetic Satellite (GEOSAT) altimeter data. The SAR geophysical products for all of these data sets were generated using manual interpretation that was subsequently digitized while the other sensor products used digital algorithms. These data sets provide the fundamental testing ground for both the analysis contained in this report as well as the analysis planned for future efforts. This data set generation is described in detail in Section 2.

Since different sensors provide the same geophysical products, the next step in our analysis was to compare them for consistency; i.e., perform algorithm verification. This was done for both total and multiyear ice concentration between the SAR and SSM/I (using the NASA algorithm), and for the ice edge location between the SAR and SSM/I. It was found that the SSM/I total ice concentration compared well with the SAR, but that the multiyear ice concentration was only accurately classifying 33% of the actual multiyear ice. In either case the variability of the SSM/I products was $\pm 15\%$. This was consistent with previous work we had performed (Jentz, 1991) where the SSM/I algorithms worked well on total ice concentration but poorly on multiyear ice; although the CEAREX data represented a different location than the previous study and thus was expected to generate different results. Errors on the order of $\pm 15\%$ are expected, so this indicated that some care must be taken in analyzing low multiyear ice concentrations. We describe below how to combine these results into a more global view of the SSM/I output products. In addition, it was found that the ice edge location was consistent between the SAR and SSM/I to within the resolution accuracy of the SSM/I. However, fusing the SAR with the SSM/I can result in improved ice edge locations due to the higher SAR resolutions. This algorithm validation is discussed in Section 3.

Having registered the geophysical products from each sensor and intercompared them, we next combined them to provide a global picture for the two CEAREX data sets; i.e., the second category of data fusion discussed above. Automated algorithms for collecting the data sets and outputing a single, comprehensive map were developed and implemented and are now available for use on future data sets. This is discussed in Section 4. A similar data fusion of sensor geophysical products was performed under an ONR contract to support analysis of the Greenland Sea tomographic array, and although it is not actually part of this program, it is a relevant example of the utility of data fusion and is included as Appendix A.

The two registered CEAREX data sets did not contain any altimeter data since the location was well north of the 72 degree inclination angle of the GEOSAT satellite, so the additional two data sets were added to allow a comparison between SAR and the GEOSAT altimeter. This analysis was begun late in the program, so to date only initial results have been generated. For the MIZEX data, the altimeter ice index values and the SAR intensity values have been registered and compared and an almost one-to-one correspondence between peaks was observed. This was shown to be consistent with previous observations that the ice index should be higher for smoother ice since a visual analysis of the SAR data showed that smoother ice corresponded to the peak SAR intensity values. Using the Alaska data, a comparison of the altimeter ice index with ice concentration showed a high correlation. Again, a visual inspection of the ice types using the SAR data confirmed the lower ice index value over the smoother ice types. These results indicate that by combining SAR and altimeter data the potential exists to provide surface roughness estimates. These results are discussed in Section 5.

As mentioned above, the ultimate goal of data fusion is to combine the raw sensor measurements to generate new unique geophysical products. One method of performing this is to use the geophysical products from one sensor to improve the

products from another. This was demonstrated using the SSM/I open water/new ice segmentation capability to improve the manual analysis of dark regions in the SAR data for which it is difficult to distinguish between open water and new ice. This showed a potential for producing more accurate high resolution ice type maps by fusing the SSM/I and SAR products. A second method to generate new geophysical products is to combine the raw sensor measurements before they are turned into geophysical products. Two analyzes were performed in this study to begin to address this question. First, the raw values from the SSM/I, AVHRR, and SAR sensors were extracted from a number of samples of known ice types. Each pair of these values were then cluster plotted with respect to each other and the mean and variance of the resulting clusters in each dimension was calculated. If the fusion of these raw measurements is to provide additional information, then the clusters from different ice types should have more separation in the two dimensions then they do in any of the one dimensions. For some of the ice types this was shown to be true, indicating a potential for data fusion. Utilizing this potential into an algorithm will be performed in the next phase. It would also be useful to use this data set to answer more global questions about data fusion; i.e., not just the separation of the specific ice types in these images. One approach is to develop a model to predict the responses of SSM/I, AVHRR, and the GEOSAT altimeter under a range of ice conditions. We have begun this analysis by using both the CEAREX data sets as well as previous work done over the Beaufort and Bering Seas to generate a series of data points that relate the SSM/I output responses to the percentage of total ice and multiyear ice within the SSM/I footprint. A model was then fit to this data to predict the SSM/I response over any ice combination within the footprint. This now provides a framework for testing data fusion over a range of ice types. Both of these analyses are discussed in Section 6.

In summary, under this initial data fusion study, we have: (1) Generated registered data sets that will be used to test the data fusion hypotheses; (2) Developed the algorithms for automatically generating spatial maps of combined geophysical products from different sensors and applied them to two CEAREX data sets; (3) Performed a comparison between the GEOSAT altimeter data and the SAR that confirmed previous results; (4) Demonstrated that the potential exists to use the SSM/I, AVHRR, and SAR sensors to distinguish ice types better than with any individual sensor; (5) Developed a SSM/I model that will allow testing of data fusion algorithms over a range of ice conditions. Obviously, this initial study does not answer the data fusion question, but has provided an initial foundation for an answer that can be built upon in future work that has been approved for funding in FY'91 and '92. Section 7 discusses in detail the framework of these future activities.

2.0 DATA SET DESCRIPTION

When determining which data set to use for this analysis it was important to find a data set that had been extensively ground truthed and one in which simultaneous sensor collections were performed. The CEAREX data collection proved to be ideal since simultaneous collections of SAR, AVHRR, and SSM/I data sets were collected along with ground truthing collected on board the ice strengthened research vessel, *Polarbjorn*. In addition to this data set, the MIZEX '87 and Alaska '88 data sets were used because of their simultaneous collections of SAR and GEOSAT radar altimeter data sets.

The SAR, AVHRR, SSM/I and altimeter sensors were chosen based on the large amount of Arctic data available (or soon to be available) for each of these sensors and because it has been shown by a number of researchers that each of these sensors alone can provide useful geophysical information about this region. Each sensor, however, has certain advantages and disadvantages which are mainly concerned with the physical phenomena that they can detect, their inherent resolution and the weather conditions through which they can operate.

The SAR has the advantage of having very high resolution and the ability to penetrate through all weather conditions. The main disadvantage of the SAR is the limited coverage area (even with the launch of ERS-1) and the large amount of processing needed to interpret the data. The SSM/I has the advantage of penetrating clouds and having global coverage, but has very poor resolution (25km). The AVHRR's resolution (1km) is one of its greatest advantages along with its large swaths, but its major disadvantage is that it cannot penetrate clouds. Finally, the GEOSAT altimeter has the advantages of being an all weather sensor and requiring a minimal amount of data processing and the disadvantage of its limited polar coverage. As shown in Figure 1 there presently exists algorithms (manual and digital) which

Geophysical Information Attainable from Sensors

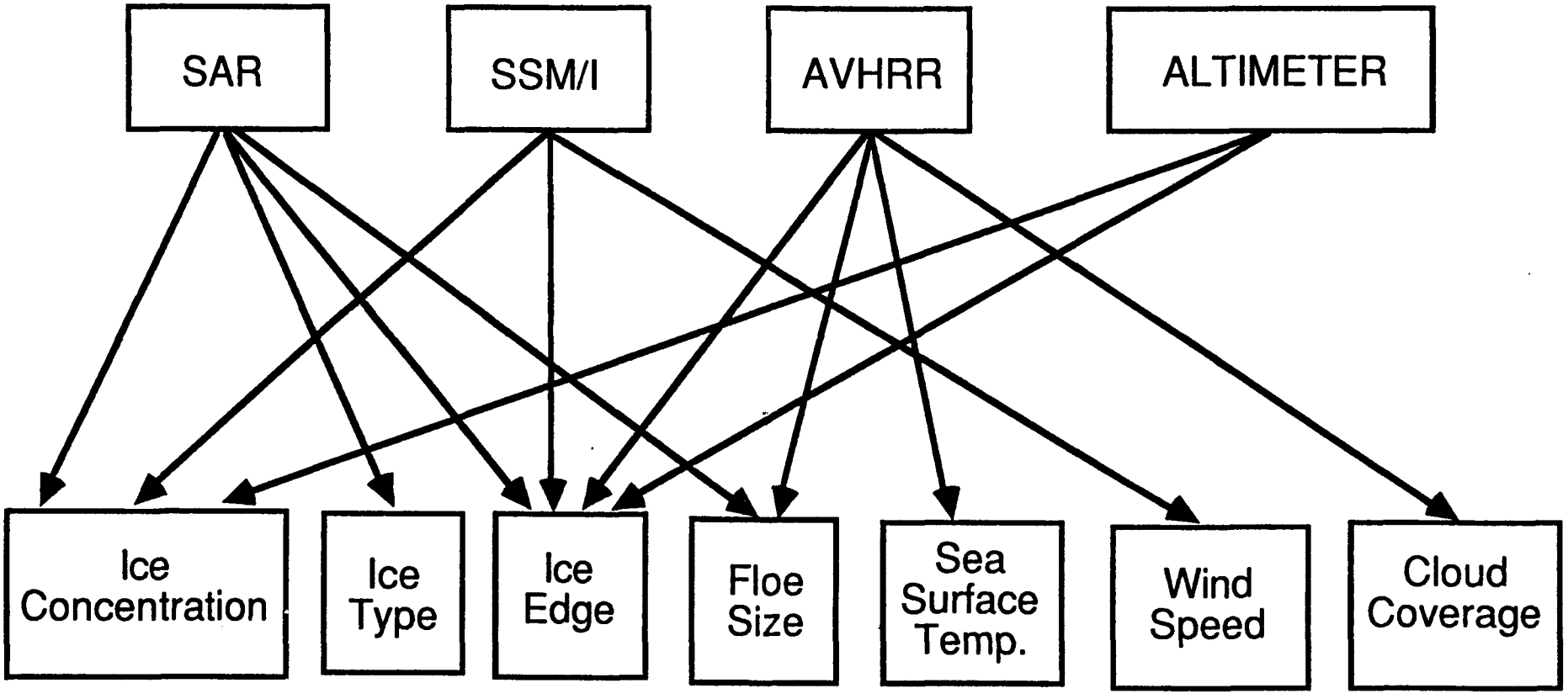

Figure 1. Summary of Geophysical Information Attainable from Various Sensors

estimate ice edge location, ice concentrations, ice type, floe size, sea surface temperature, wind speed and cloud coverage over the Arctic oceans for each of these sensors. A summary of this information is presented in Table 1.

2.1 DATA REGISTRATION

In order to "fuse" the data described above it was necessary to register each of the data sets to do a pixel-by-pixel comparison. The 17 and 20 March 1989 data sets are representative of the nine coincident SAR, SSM/I, and AVHRR data sets collected during CEAREX and were therefore used for this data fusion analysis. For both of these dates each of the sensors collected data in the Greenland Sea MIZ centered at about 77° N Latitude and 0° longitude. To perform the registration each of the sensor data products were resampled on a common 5 km grid spacing and common map projection.

The SAR data used in this analysis has a resolution of about 3 meters and a wavelength of 5.6 cm (C-Band) with vertical transmit and receive polarization. This configuration of wavelength and polarization was chosen because the ERS-1 has the same configuration. The digital SAR data was optically processed and mosaiced together to form images of the arctic region, as shown in Figures 2 and 3. In order to generate this common grid, the SAR mosaics were manually interpreted on a 5 km grid to extract ice concentration, multiyear fraction, floe size, lead and ridge statistics. Each grid point was then assigned a latitude and longitude value and the rest of the data sets were registered based on the SAR data's map projection. These manual interpretations of the SAR data have an error of $\pm 5\%$ as found by comparing the manual interpretations of three different researchers.

The SSM/I algorithms produce data on a 25 km grid spacing in a polar stereographic projection. This data was first upsampled to a 5 km spacing using a

Table 1. Summary of Satellite Sea Ice Data Sources

Satellite	Sensor	Type	Swath (Km)	Resolution	Revisit Time/Day	Sea Ice and Ocean Parameters Measured	Advantage	Disadvantage	Status
Landsat	Multi-spectral Scanner (MSS)	Passive Visible and Infrared	186 x 186	30 m	0	Ice edge, ice concentration, floe size distribution, ice motion, chlorophyll concentration, suspended sediment, location of ocean fronts	High resolution information is easily extracted	Clouds, coverage limited to 81°	Operational
Spot	Multi-spectral Scanner (MSS)	Passive Visible and Infrared	60 x 60	10 m	0 - 2	Ice edge, ice concentration, floe size distribution, ice motion, chlorophyll concentration, suspended sediment, location of ocean fronts	High resolution information is easily extracted	Clouds, coverage limited to 81°	Operational
DMSP	Optical line Scanner (OLS)	Passive Visible and Infrared	2900	0.6 - 3 Km	2 - 12	Meteorology, ice motion, ice edge location, eddy structure, sea surface temperature, ice kinematics	Large swath	Clouds	Operational
DMSP	Special Scanning Microwave Imager (SSM/I)	Passive Microwave	750	50 - 60 Km	0 - 2	Ice type, ice extent, ice concentration, eddy structure, water vapor, and ocean surface winds, sea surface temperature	Penetrates clouds	Resolution, melt & freeze period	Operational
NOAA 9/10	Advanced Very High Resolution Radiometer (AVHRR)	Passive Visible and Infrared	2500	1 - 4 Km	2 - 12	See DMSP OLS	Large swath	Clouds	Operational
GEOSAT	Radar Altimeter	Active Microwave	Nadir Profile 7 -10	height 10 cm spot size 7 - 10 Km	0	Ice edge, ice roughness, gravity wave detection, ice concentration, ocean height topography, geostrophic currents	All weather minimum data processing	Limited polar coverage, profile only, large spot size	Operational
Japanese MOS-1	Multi-spectral Electronic Self Scanning Radiometer (MESSR)	Passive Visible and Infrared	200	50 m	0	See LANDSAT MSS	High resolution information is easily extracted	Clouds	Operational
Japanese MOS-1	Visible and Thermal Infrared Radiometer (VTIR)	Passive Visible and Infrared	1,500	1 - 3 Km	2 - 12	See DMSP OLS	Large swath	Clouds	Operational
Japanese MOS-1	Microwave Scanning Radiometer (MSR)	Passive Microwave	300	30 - 40 Km	0 - 1	See DMSP SSM/I	Penetrates clouds	Resolution, melt and freeze period	Operational
ESA ERS-1	Radar Altimeter	Active Microwave	Nadir Profile 7 -10	height 10 cm spot size 7 - 10 Km	0	Ice edge, ice roughness, gravity wave detection, ice concentration, ocean height topography, geostrophic currents	All weather minimum data processing	Profile only large spot size	Proposed launch Mid 1991
ESA ERS-1	Synthetic Aperture Radar (SAR)	Active Microwave (C-band)	80 - 100	30 m	0	Ice edge location, eddy and ocean front structure, ice type, floe size distribution, ice kinematics, gravity wave propagation, internal wave measurements, ice concentration, surface wind speed, detection of leads, mapping of icebergs	All weather high resolution	Coverage, data processing	Proposed launch Mid 1991

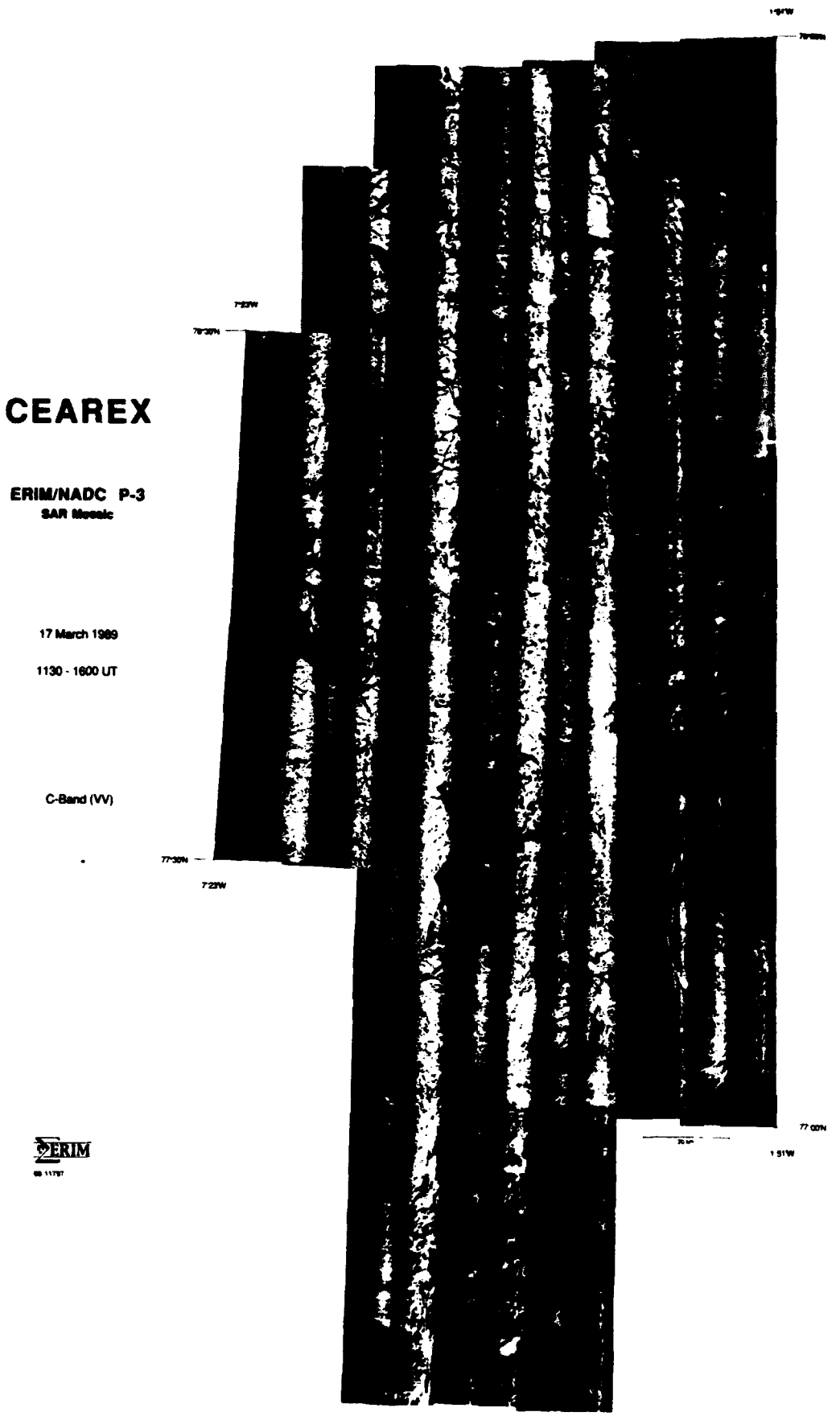

Figure 2. Optically Processed Mosaic of SAR Data Collected During CEAREX, 17 March 1989

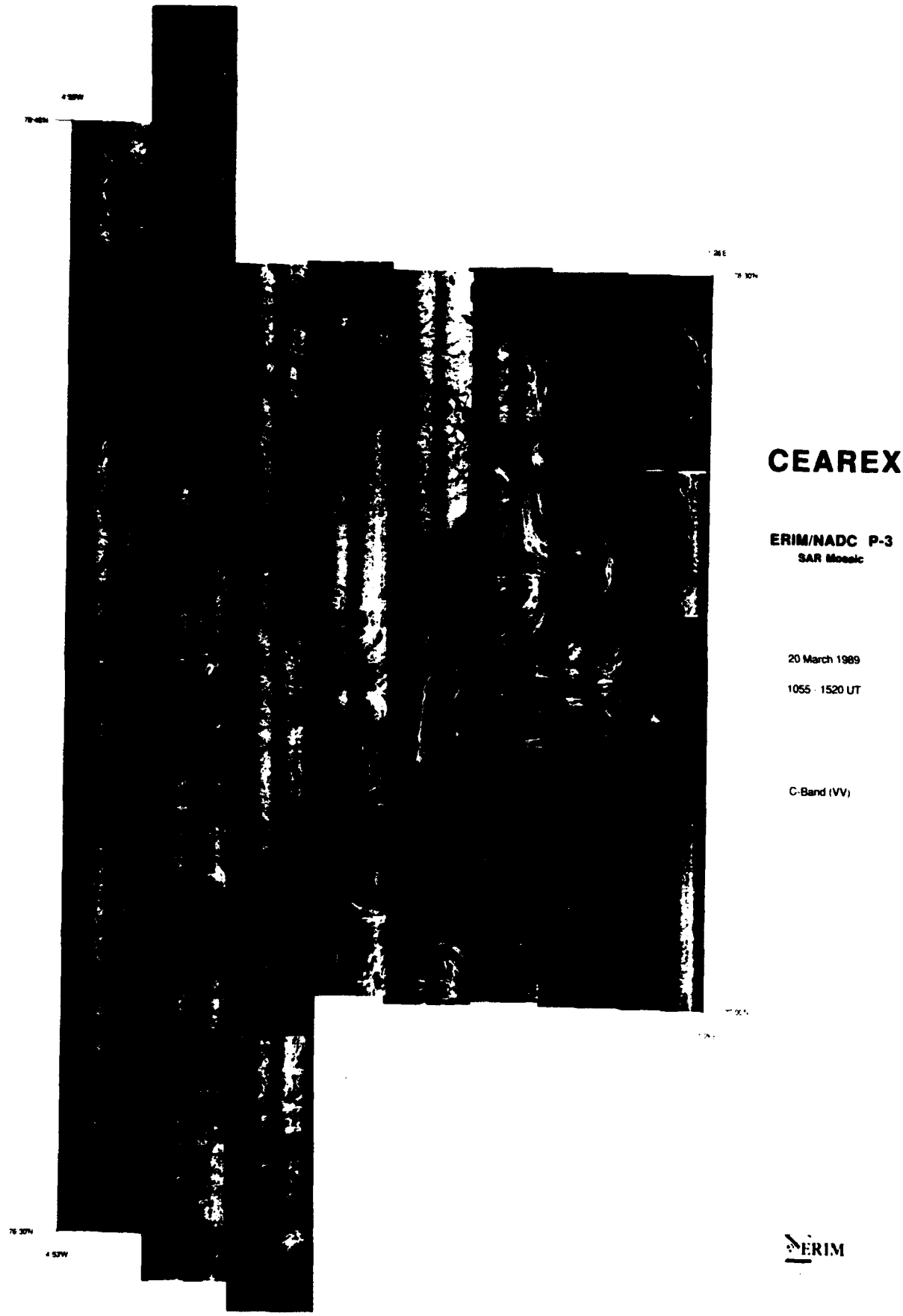

Figure 3. Optically Processed Mosaic of SAR Data Collected During CEAREX, 20 March 1989

bilinear interpolation technique. The latitude and longitude values for each point were also upsampled to a 5 km spacing so that each pixel would have an associated latitude/longitude value. The data was then converted to the SAR 5 km map projection by assigning an interpolated SSM/I data value to each of the SAR grid points based on the latitude and longitude values derived for the sensor. Because the coverage of the SSM/I data was much greater than that of the SAR mosaic, the SSM/I data which included the mosaic region was used along with the SSM/I data values surrounding the mosaic so as to get a more global picture of the study region. The actual algorithms used to generate the SSM/I products are discussed in Section 4.

The AVHRR data used for this analysis was the Local Area Coverage (LAC) 1 km resolution data. In order to use this data on the same grid as the SAR and SSM/I, it needed to be downsampled to a 5 km grid. To do this, the data was resampled at a 5 km spacing by performing a 5 by 5 pixel averaging and the center pixel was replaced by the average. This was done on both the data files and on the latitude/longitude grids so as to give a data value and latitude/longitude location for each pixel in the image. Like the SSM/I data sets, the data was then converted to the SAR 5 km map projection by assigning a downsampled AVHRR data value to each of the SAR grid points based on the latitude and longitude values derived for the sensor. As with the SSM/I, the AVHRR data which included the mosaic region was used along with the AVHRR data values surrounding the mosaic so as to get a more global picture of the study region. The actual algorithms used to generate the geophysical output products from the AVHRR are discussed in Section 4.

The GEOSAT altimeter collects data only as far north as 72 degrees latitude, therefore, we were not able to use this data in the fusion of CEAREX data sets. There was, however, altimeter data available which corresponded to one SAR mosaic from the Alaska '88 collection (March 21, 1988) and a SAR dedicated GEOSAT underflight collected during the MIZEX '87 collection. In order to register the SAR

and altimeter data sets collected during the Alaska '88 data collection, the limited number of altimeter data points were mapped onto the SAR mosaic and the percentage of total ice concentration was manually derived from the SAR for each of the altimeter footprints. For the MIZEX '87 underflight the SAR data was digitized and average intensities were calculated (within the footprint of the altimeter footprint) for the entire altimeter flight path. A direct comparison of the SAR and altimeter data sets could then be made by simply noting the starting and ending latitude and longitude for the SAR underflight as compared to those noted by the GEOSAT.

3.0 ALGORITHM VERIFICATION USING DATA FUSION

As shown in Figure 1, there is much overlap between the geophysical products estimated by different sensors, and when combining them, the consistency of estimates between sensors needs to be checked. Often one sensor will generate a more reliable estimate than another, and thus can become the "truth" against which the less reliable algorithm is verified. Such algorithm verification using data fusion can be very useful, since independent confirmation of ice concentrations or ice edge location, for example, over the hundreds of kilometers that the satellite sensors image is practically impossible; such sensor intercomparisons may be the only algorithm checks that can be performed. Typically the higher resolution sensors can generate the more reliable estimates since they can be manually interpreted easily, and thus provide the verification for the coarser resolution sensors. The SAR data provided far and away the best resolution of the sensors used in this study and thus was used to verify the results from SSM/I.

The results of the SSM/I NASA ice concentration algorithm (see Section 4 for a discussion of the SSM/I algorithms used in this study) were validated using the SAR manual interpretation as ground truth. In order to perform this task the registered 17 and 20 March CEAREX SAR and SSM/I data sets were used. Various positions in the imagery were selected and both the total and multiyear concentrations were noted for the SAR and SSM/I. The results were plotted for each of the dates and are shown in Figures 4 through 7. The closer the data points lie to a 45 degree angle in the plots, the better the algorithm performs since this represents an exact match between the SAR and SSM/I estimates. Figures 4 and 6 show that the NASA algorithm is a good predictor of total ice concentration. A line fit to the data is very close to the 45 degree line, and the cluster about that line is approximately $\pm 15\%$ for March 17 and $\pm 20\%$ for March 20. This is consistent with previous studies (Cavalieri, 1990)

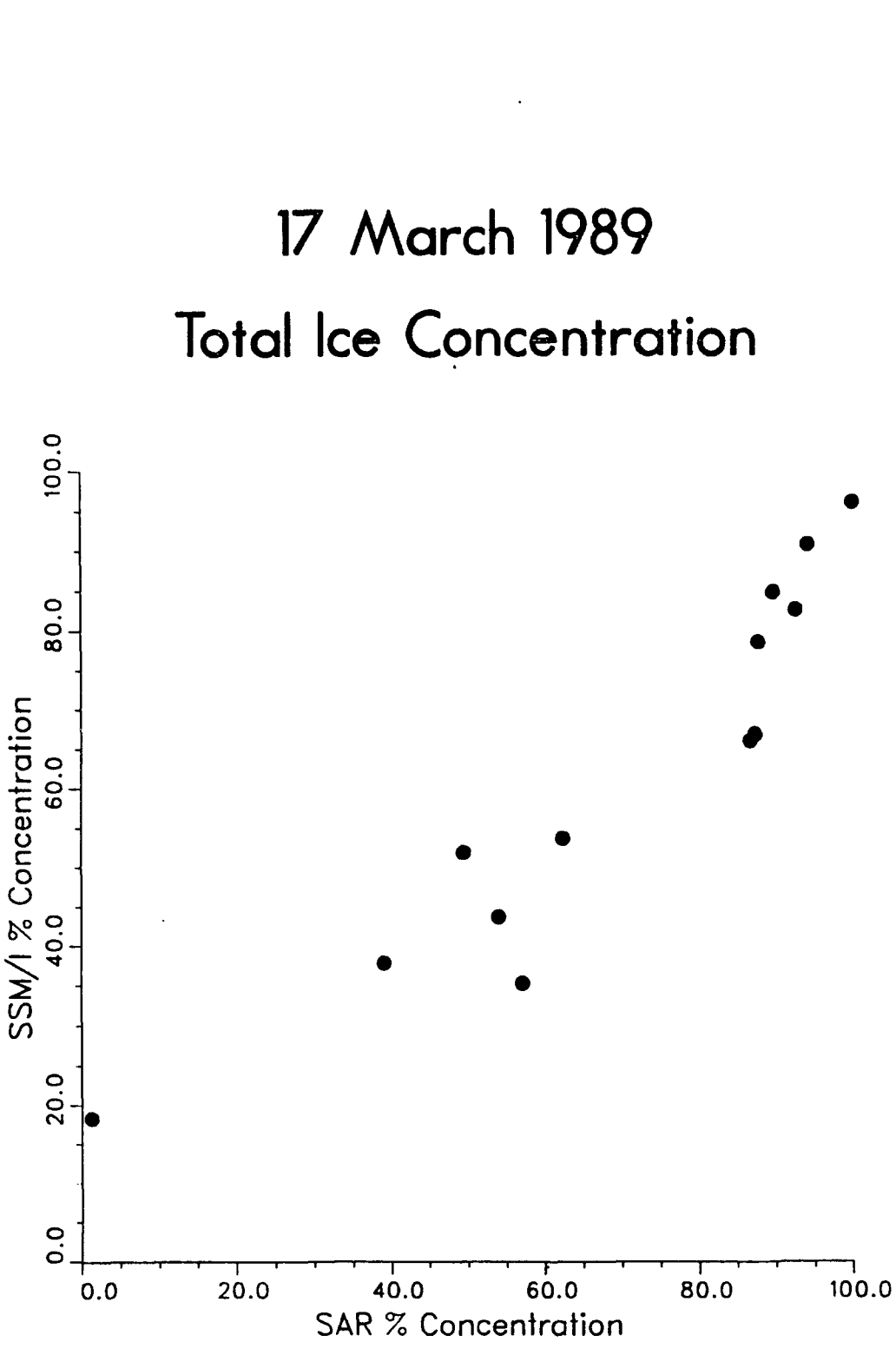

Figure 4. Plot of SAR Total Ice Concentration versus SSM/I Derived Total Ice Concentration for 17 March 1989

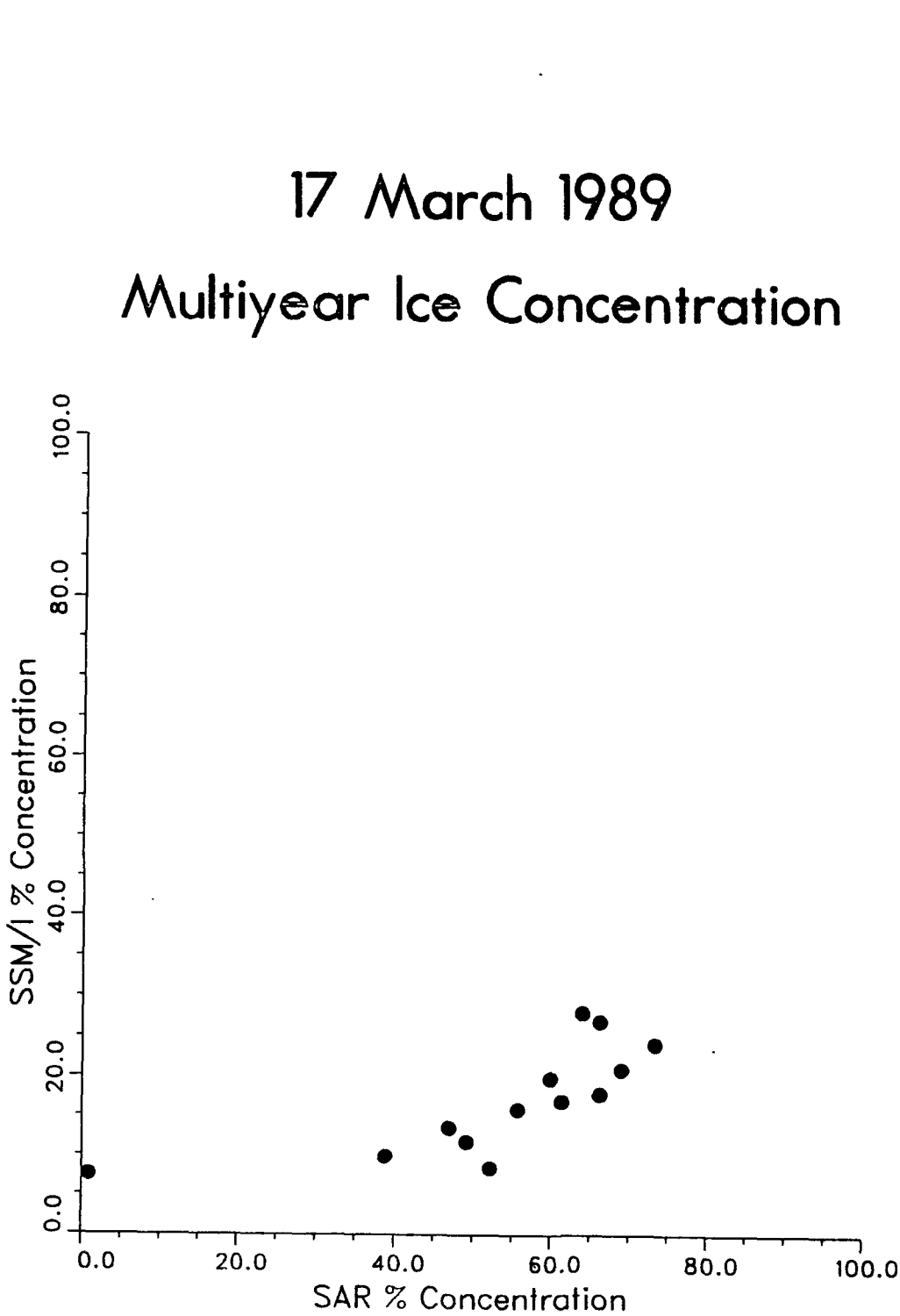

Figure 5. Plot of SAR Multiyear Ice Concentration versus SSM/I Derived Multiyear Ice Concentration for 17 March 1989

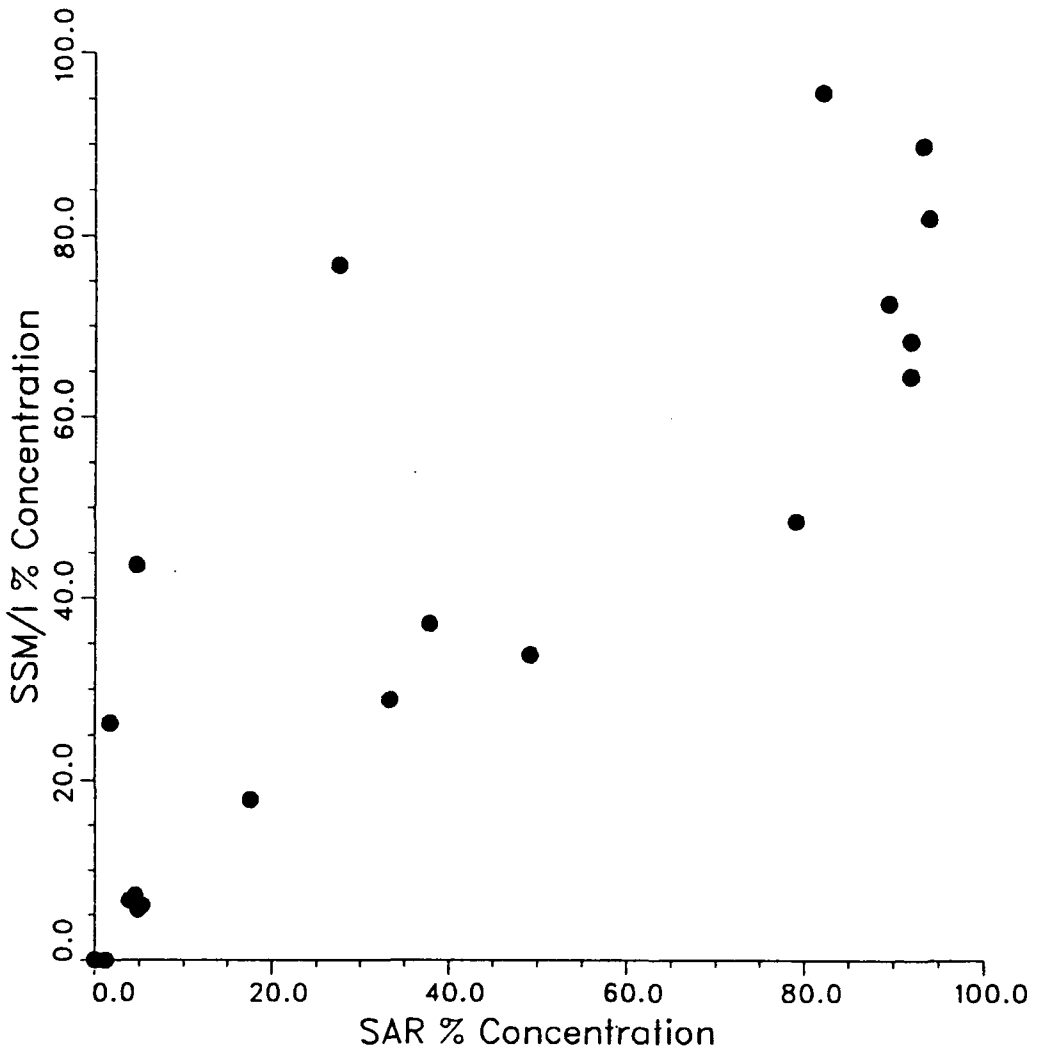

Figure 6. Plot of SAR Total Ice Concentration versus SSM/I Derived Total Ice Concentration for 20 March 1989

20 March 1989

Multiyear Ice Concentration

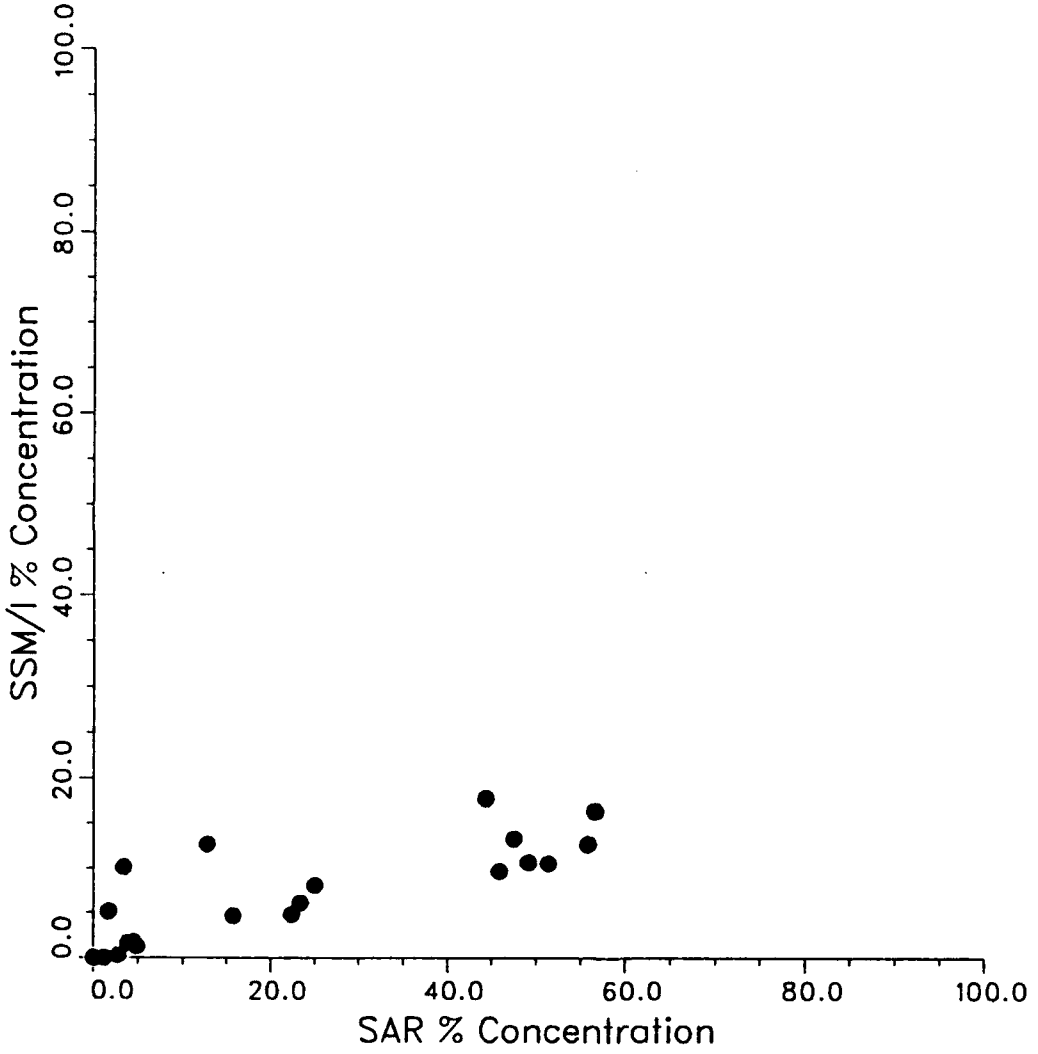

Figure 7. Plot of SAR Multiyear Ice Concentration versus SSM/I Derived Multiyear Ice Concentration for 20 March 1989

which show that the SSM/I variations were approximately ±13%; although the March 20 data is a little high. The algorithm is not, however, as good of a predictor of multiyear ice concentration, as shown in Figures 5 and 7. The fit line to this data has a slope of approximately 0.33 for both cases instead of 1.0; although the cluster about the line is somewhat tighter, approximately ±10%. This indicates that the SSM/I is underpredicting the multiyear ice concentration and thus, since it is predicting the total ice concentration adequately, over predicting the amount of first year ice. In fact, the slope of 0.33 indicates that only 33% of the multiyear ice is being classified as such with 67% being classified as first year. The rapid fluctuations of ice concentrations within this region may have contributed to this error, although it appears that this discrepancy is worth further investigation. However, since it represents a sideline to this fusion study, it was not pursued further.

Another type of validation that can be performed on this data set is the validation of ice edge location between sensors. This can be easily performed by examining a composite imagery of SAR and SSM/I data where the SAR data is overlapped on top of the SSM/I (this will be discussed later in Section 4 and are shown as Figures 14 and 15). Since it has been commonly accepted that the SSM/I 20% concentration line is closer to the actual ice edge than the 0% line, this was used in the comparison. It was found that the SSM/I ice edge is off by about 35 km for the March 17 data. Since the SSM/I has a resolution of 25 km this is not surprising since there will be an inherent error of ±25 km in the data to start with, and upsampling to a 5 km grid will add additional error. Another possible source of error is that a bilinear interpolation was performed on the data (which assumes a linear variation between the data points) and at this location of the ice edge the concentration levels are not linear; they change quickly from 100% ice to 0% ice, which could not have been predicted with a bilinear interpolation technique. The SSM/I derived ice edge in the March 20 data is much closer to the actual concentration line (within about 5km) than the

previous figure. This may be due to the fact that the concentration amount is changing much less rapidly as it moves into the open ocean than it did in the previous image. In general, the ice edge locations between the SAR and the SSM/I appear consistent given the data sampling and interpolation schemes used.

This verification of sensor products proved to be a necessary first step in this study. It was essential in understanding that the SSM/I can be a good predictor of total ice concentration in data fusion, but one must be cautious and more effort must go into the derivation of multiyear concentration levels with this sensor. It was also shown that the SSM/I is a good predictor of ice edge when taking its poor resolution into account.

4.0 GENERATING COMPOSITE PICTURES

With multiple sensors imaging the same location and generating multiple geophysical estimates, it is possible for one to combine the sensor outputs to generate a more useful description of the scene. While such "data fusion" has been going on manually for years, performing this process digitally, as well as automating it to increase product generation, and utilizing additional sensors such as satellite based active microwave SARs and the GEOSAT altimeter are areas of research. The difficulty is the development of reliable, automatic algorithms that utilize the sensor data to extract geophysical estimates.

As shown in Figure 1, algorithms have been developed to derive various geophysical estimates from the SAR, SSM/I, AVHRR and GEOSAT altimeter. The combination of all of the geophysical estimates indicated in Figure 1 can provide a more complete description of the scene being imaged than any one sensor can provide alone. This has routinely been performed manually with a limited number of sensors in the past to provide Arctic sea ice charts. With the continued increase in digital algorithms to extract geophysical information and the continued increase in the quantity of available data, it is becoming necessary to automate this process to decrease product generation time as well as incorporate these new algorithms.

4.1 DEVELOPING COMPOSITE IMAGES

The first step in developing these composite images was to register the output products from each sensor; i.e., map output samples from each sensor onto a common grid. This was discussed in detail in Section 2.1 of this report. This registration procedure was performed on both the 17 and 20 March 1989 data sets for the SAR, SSM/I and AVHRR. Figures 8 through 10 show the output products from this

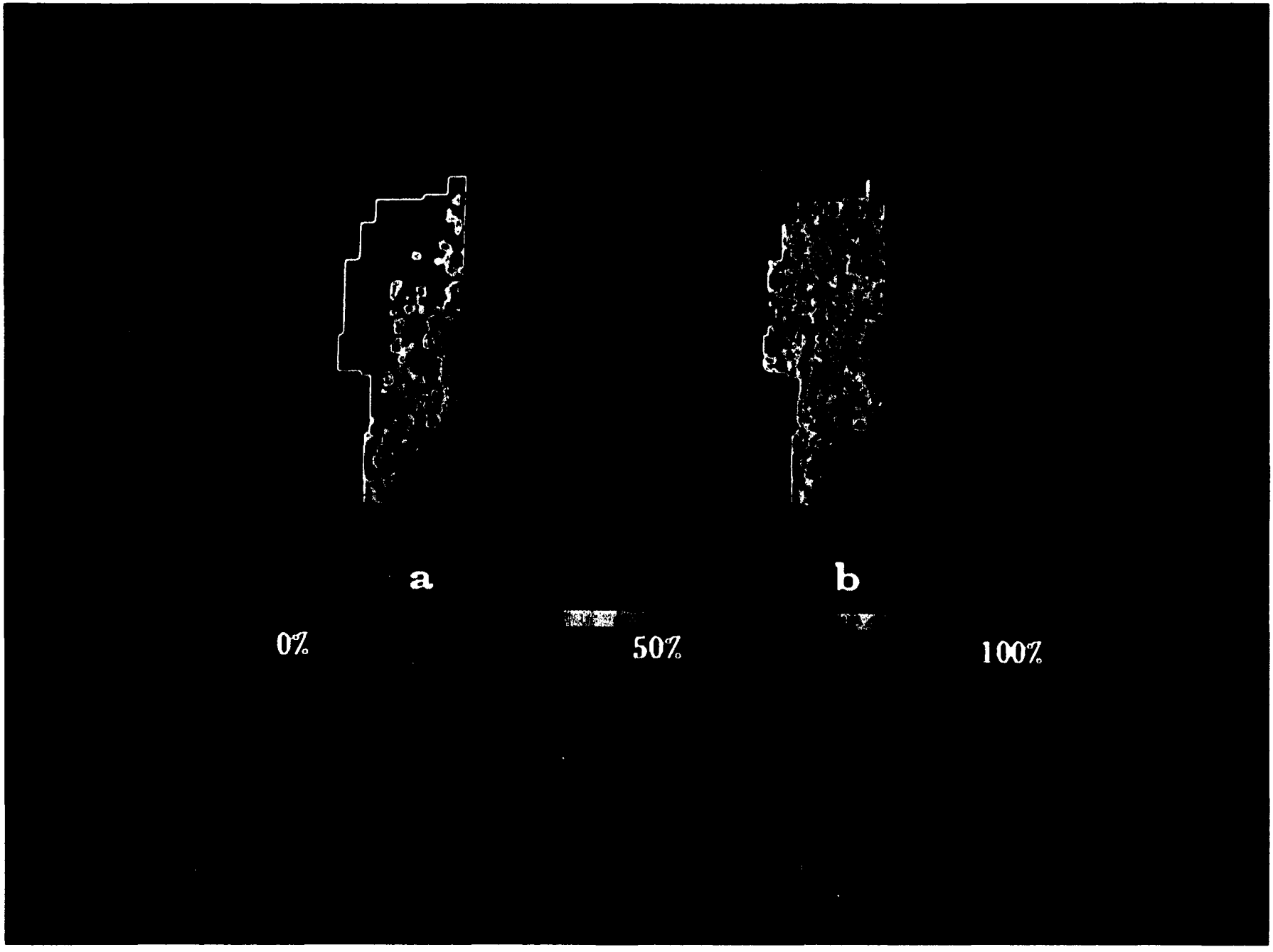

Figure 8. SAR Derived Data Products for 17 March 1989, (a) Total Ice Concentration and (b) Multiyear Ice Concentration

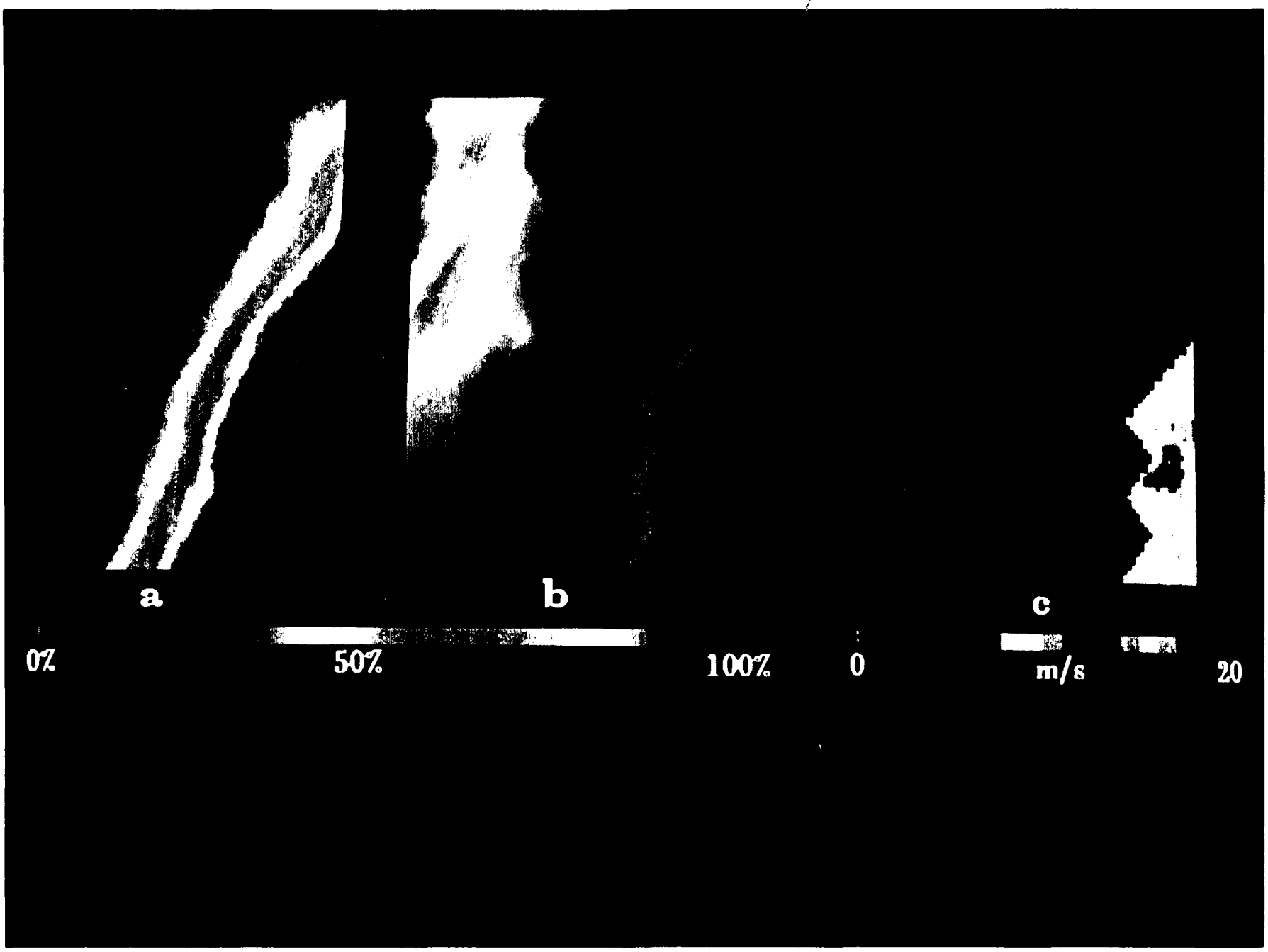

Figure 9. SSM/I Derived Data Products for 17 March 1989, (a) Total Ice Concentration, (b) Multiyear Ice Concentration and (c) Near Surface Wind Speed

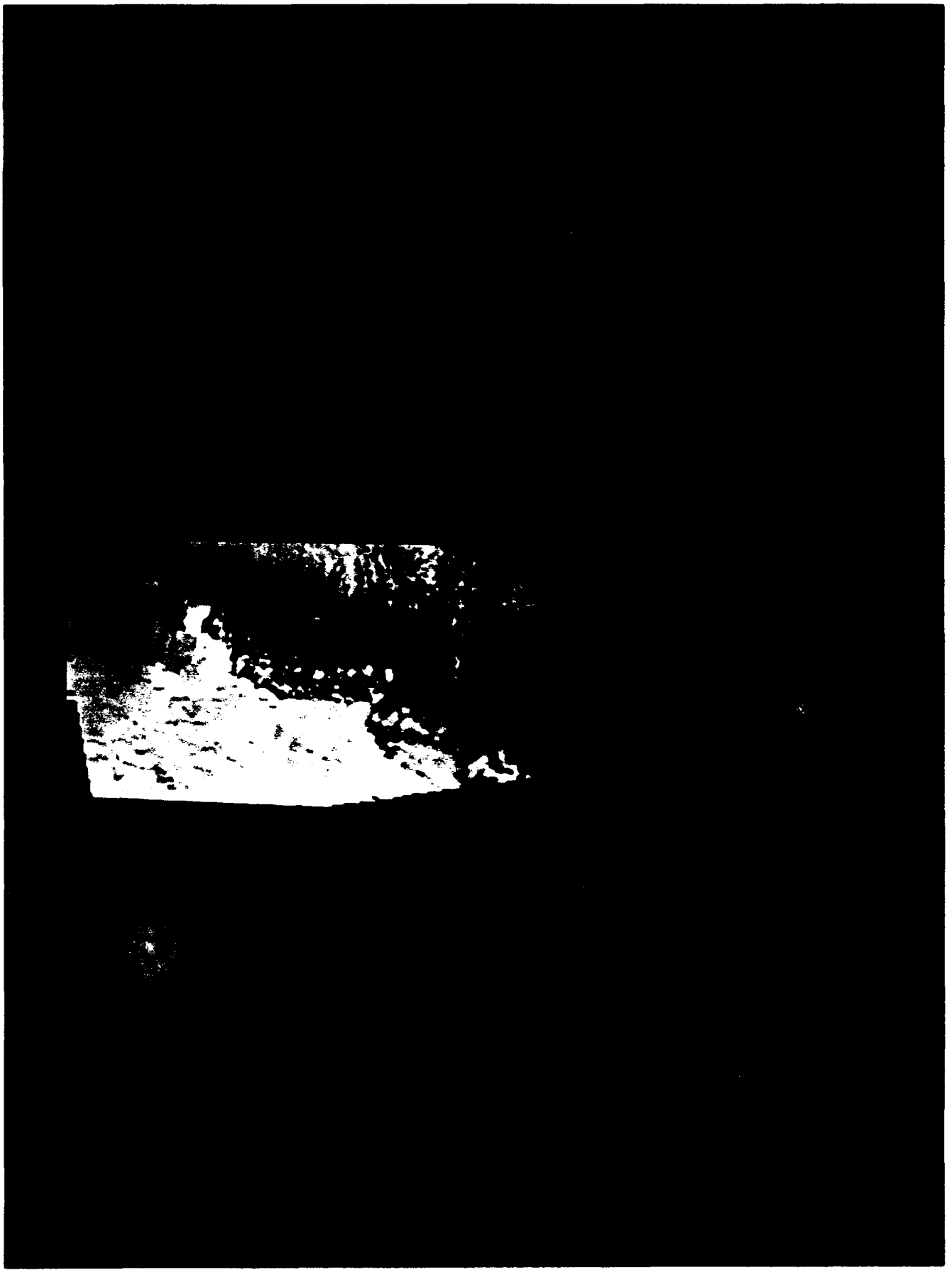

Figure 10. AVHRR Visible Channel for 17 March 1989

registration performed on the 17 March data set. Figures 11 through 13 show the output products for the 20 March data set.

Figures 8 and 11 show the SAR output products of total ice concentration (a) and multiyear ice concentration (b) where the color indicates the percentage of ice. The color bar at the bottom shows how to translate the colors into percentages. Each of these concentration estimates were derived using a manual interpretation of the optically processed data (with an error of ±5%) on a 5 km grid.

Figures 9 and 12 show the SSM/I products of total ice concentration (a), multiyear ice concentration (b) and near surface wind speed (c). The ice concentration estimates were derived on a 25 km grid using the algorithm adopted by the NASA Sea Ice Algorithm Working Group (Gloersen et al., 1986). The data for these algorithms were obtained from the SSM/I brightness temperatures (TB's) supplied on CD-ROM from the National Snow and Ice Data Center (NSIDC). The CD-ROM's contain Tb's binned on a 12.5 km grid for the 85 GHz channels and on a 25.0 km grid for the 19, 22, and 37 GHz channels. The Tb's were averaged over a 24 hour period (midnight to midnight) to produce one gridded brightness temperature map per day for each of the seven SSM/I channels. The NASA ice concentration algorithm uses three of these gridded brightness temperature channels: 19 GHz vertical, 19 GHz horizontal, and 37 GHz vertical to calculate total and multiyear ice concentrations. The algorithm assigns each grid cell a percent total and percent multiyear ice concentration (0 - 100%) based on the three Tb's. While a number of other algorithms exist which convert the SSM/I brightness temperatures into ice concentration (Jentz, 1991), the software distributed with the CD-ROM's contained the NASA ice concentration algorithms and was therefore used to generate both the total and multiyear ice concentrations.

The derivation of the near surface wind speed was performed using a Navy algorithm (Hollinger, 1989) with the same CD-ROM data set. This algorithm uses

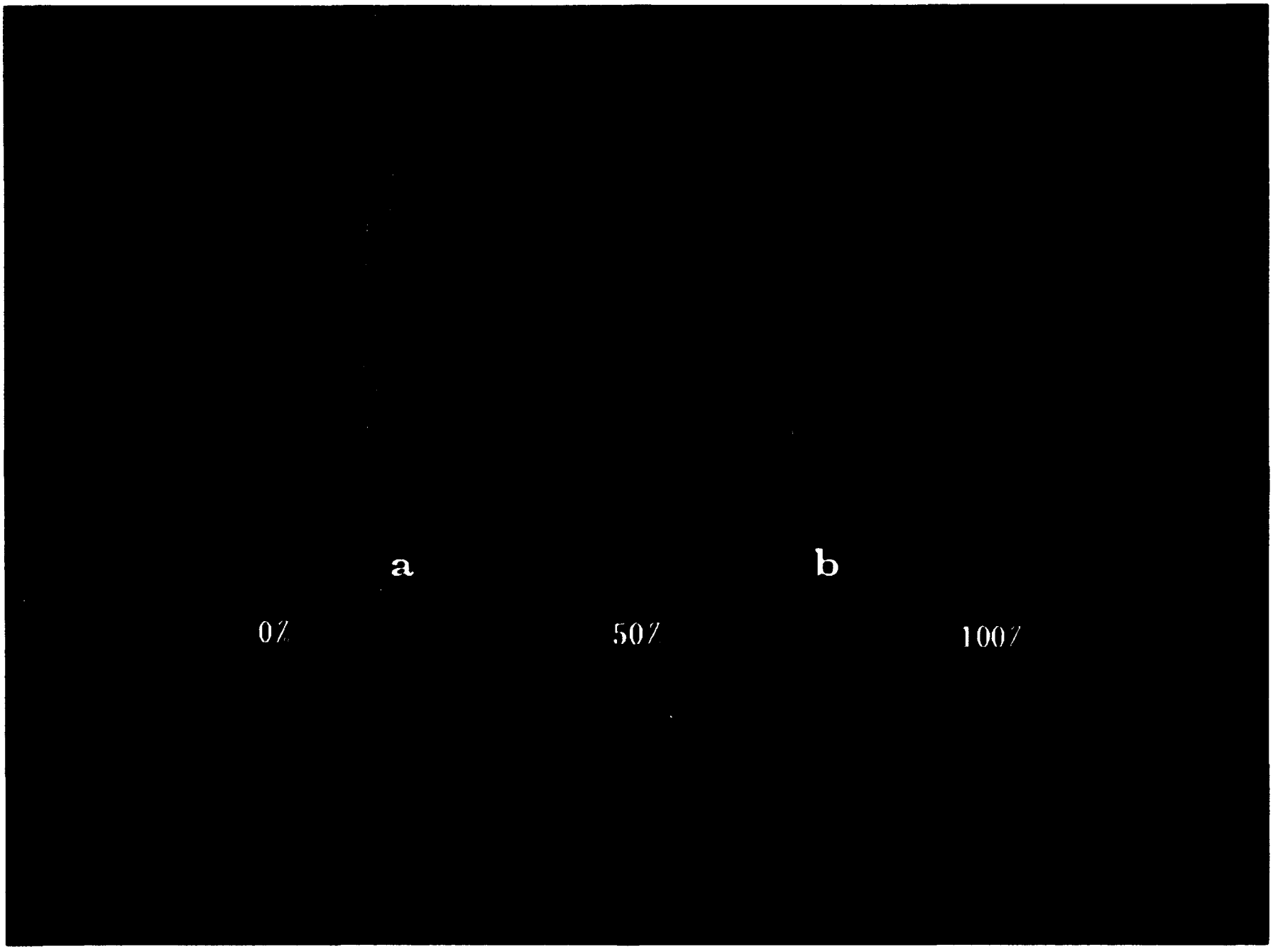

Figure 11. SAR Derived Data Products for 20 March 1989, (a) Total Ice Concentration and (b) Multiyear Ice Concentration

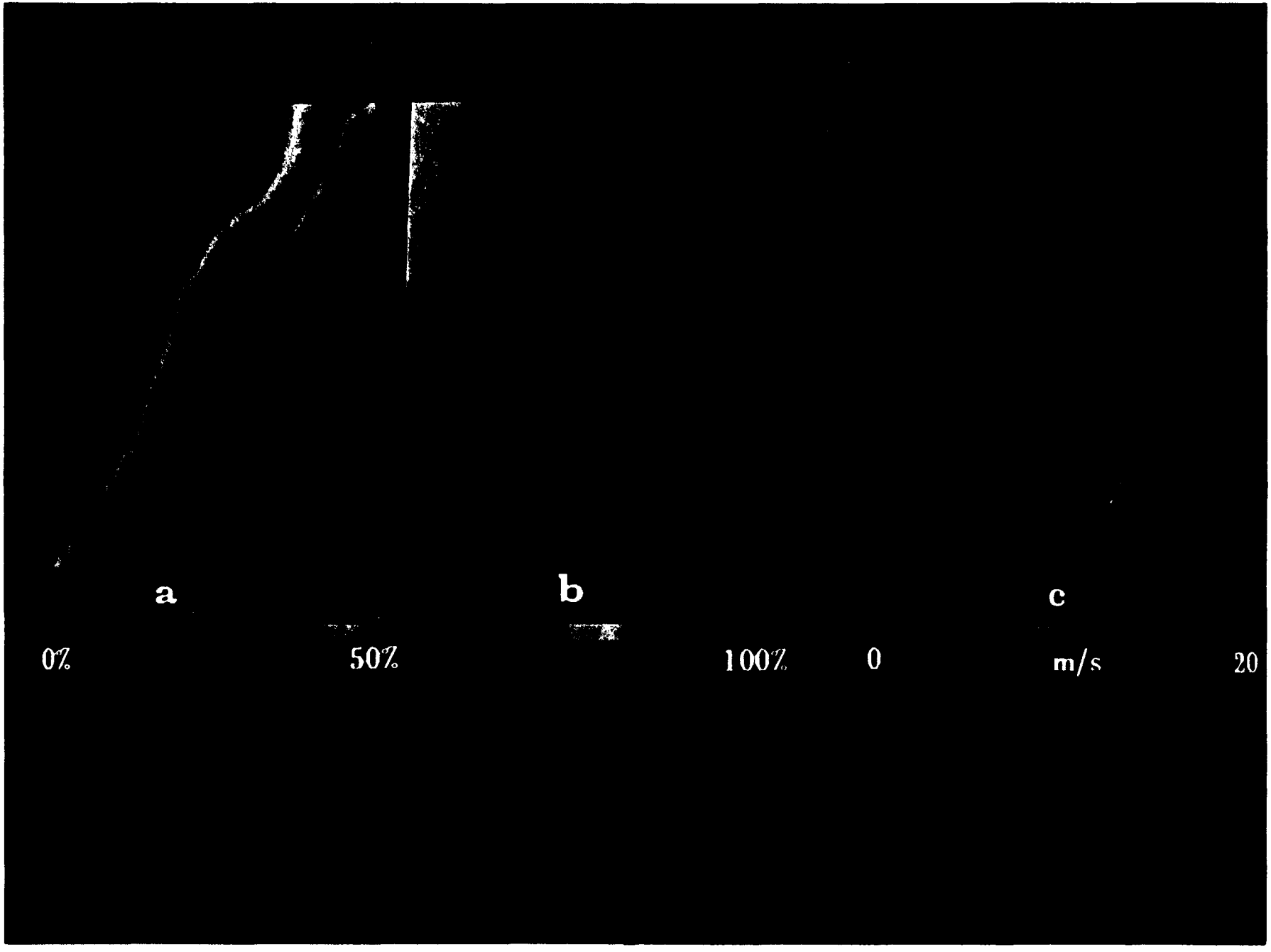

Figure 12. SSM/I Derived Data Products for 20 March 1989, (a) Total Ice Concentration, (b) Multiyear Ice Concentration, and (c) Near Surface Wind Speed

the following SSM/I brightness temperatures to calculate an estimate of the near surface wind speed: 19 GHz V and H, 22 GHz V, and 37 GHz V and H. This algorithm calculates the near surface wind speed in meters/seconds and is only valid in open water areas. The ice covered areas were flagged as bad data points.

Figures 10 and 13 show the AVHRR visible products from channel 2 (a) and (in Figure 13 only) the derived sea surface temperature from channel 4 (b). The visible data product is simply a scaled version of the visible channel which easily shows the ice/water boundary and floe location. The sea surface temperature was derived using a linear conversion from the infrared brightness temperature (channel 4) to degrees celsius as described during a conversation with Jeff Hawkins of Naval Oceanographic and Atmospheric Research Laboratory (NOARL). Since the AVHRR cannot penetrate clouds and since the clouds will cause a great deal of variation in the temperature, sea surface temperature was not calculated for the March 17 data set which had heavy cloud coverage.

Algorithms were developed to automatically combine the geophysical outputs from each sensor onto a single spatial map. In order to represent the various geophysical products simultaneously, color was used for total ice concentration, overlaid contours for sea surface temperature and arrows for wind conditions (where wind direction was generated on the *Polarbjorn)*. The resulting composite maps for the two CEAREX data sets are shown in Figures 14 and 15. The composite view in Figure 14 describes total ice concentration (color), wind conditions (arrows), and sea surface temperature (contours) for the 20 March data set. The composite view in Figure 15 describes total ice concentration (color) and wind conditions (arrows) for the 17 March data set, but because of the heavy cloud coverage, sea surface temperature could not be derived. Therefore, low clouds are represented by the heavy crosshatching and high clouds are represented by the lighter crosshatching.

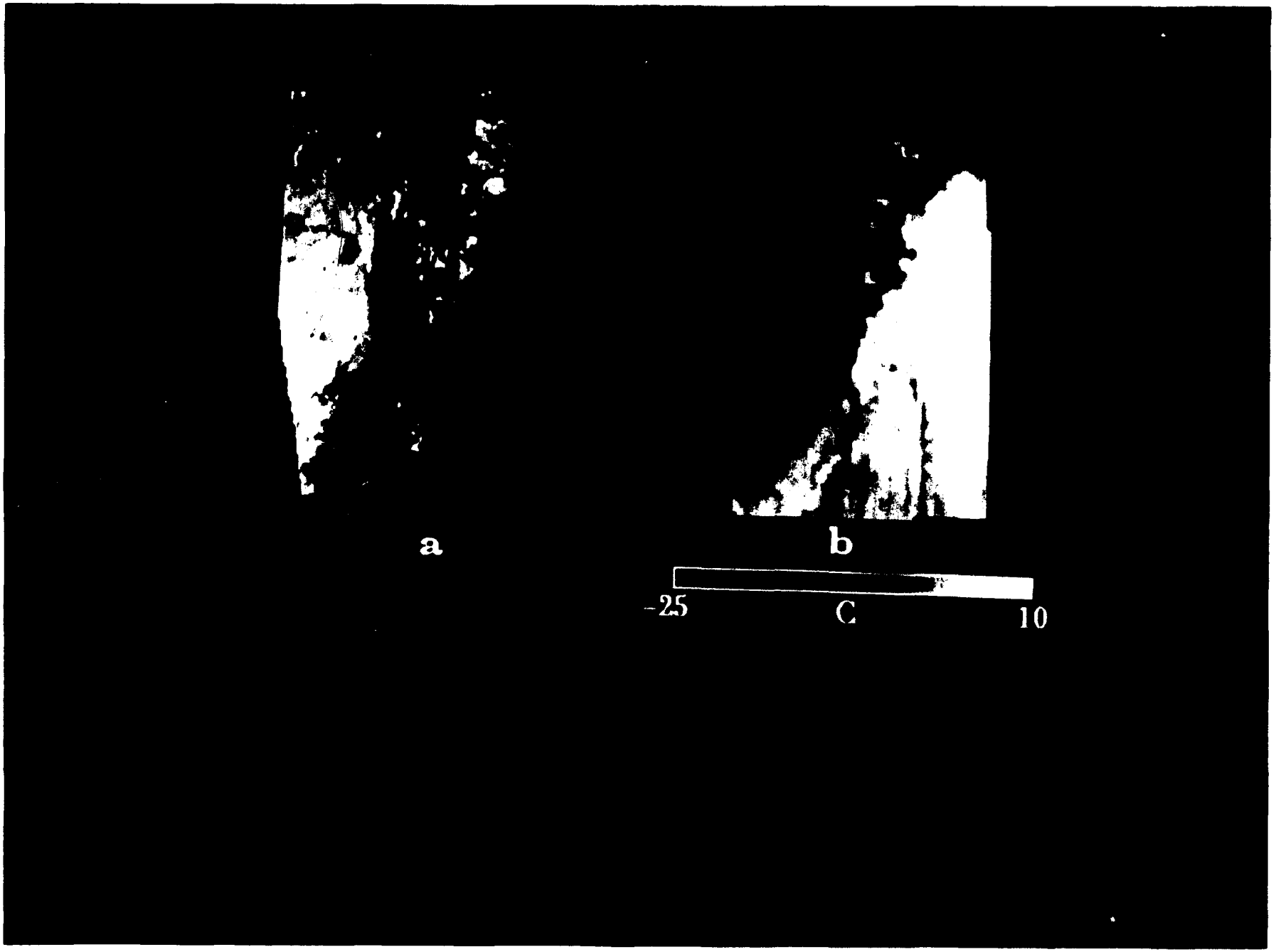

Figure 13. AVHRR Derived Data Products for 20 March 1989, (a) Visible Channel and (b) Sea Surface Temperature

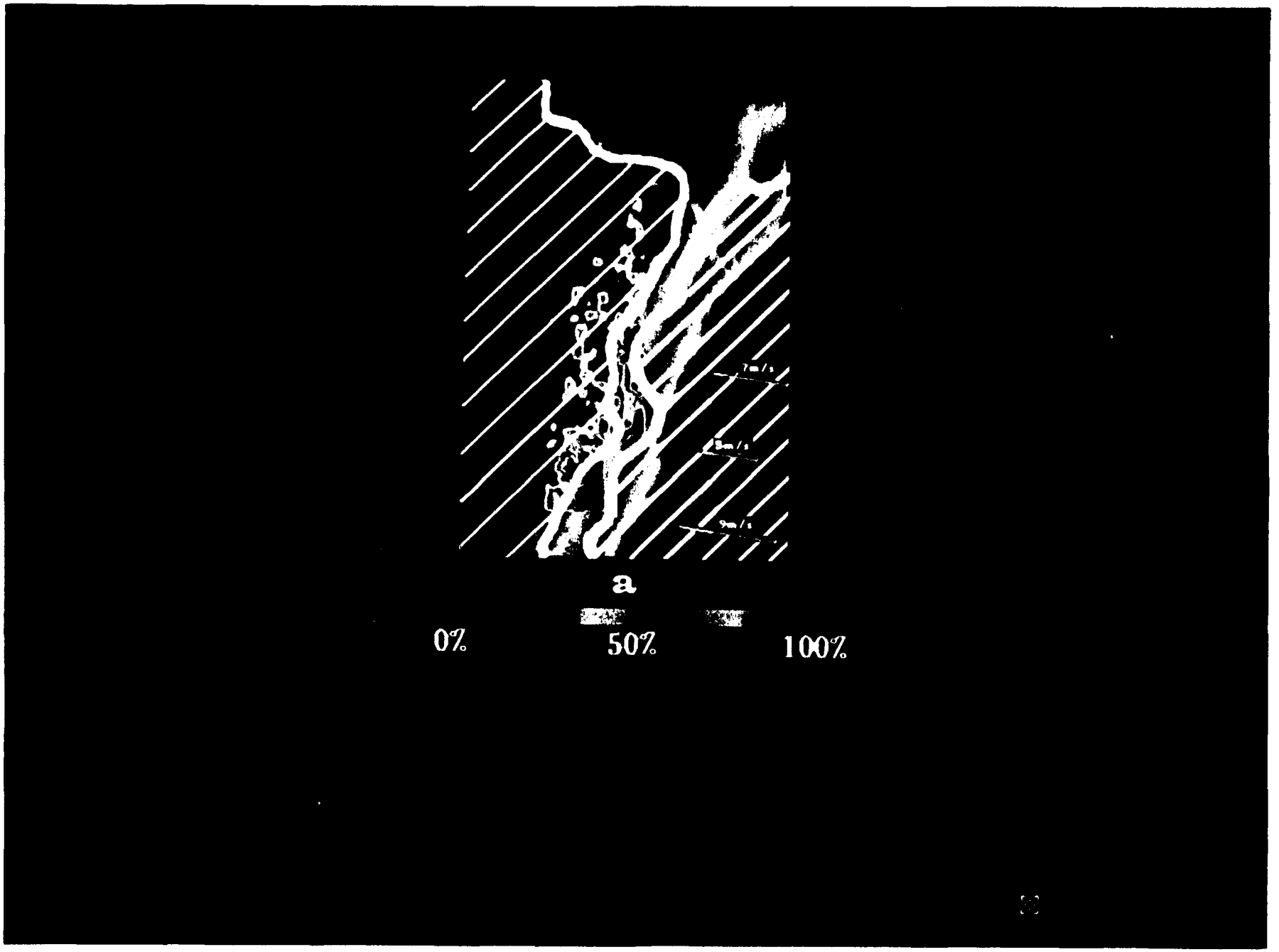

Figure 14. Composite Image of SAR, AVHRR and SSM/I Data Products for 17 March 1989

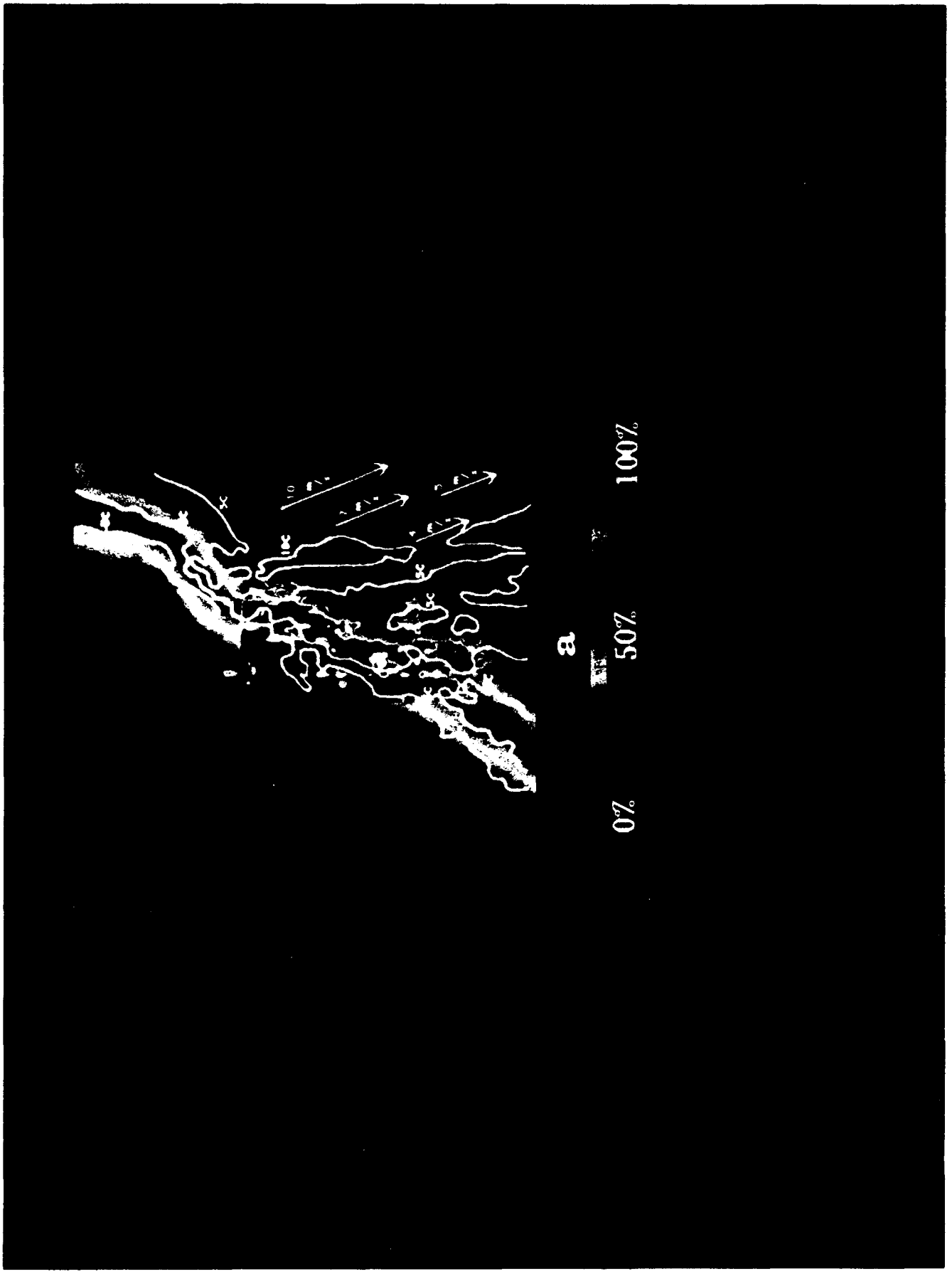

Figure 15. Composite Image of SAR, AVHRR and SSM/I Data Products for 20 March 1989

It is difficult not to use these composite images for algorithm validation. As mentioned in Section 3 above, comparisons of the ice edge location between SAR and SSM/I can easily be done with these images. In addition, using Figure 15 a comparison between SSM/I ice concentration and sea surface temperature shows that the 40 to 50% concentration lines appear to follow the 0 degree contour more accurately than other concentrations. However, the dominant use of these composite maps is to simultaneously display, for a given spatial location, the ice concentration, temperature, cloud coverage, etc. of the environment. These data compilations are invaluable when analyzing other data sets that can be effected by these environmental conditions since it can show the simultaneous effects of different conditions; ice thickness and cloud cover may both effect heat flow calculations, or wind speed and ice roughness may both effect wind friction. In fact, under a different study a similar geophysical product compilation was performed to support the analysis of acoustic properties recorded during the Acoustic Tomography Experiment and was found to be very useful to the researchers in reconstructing the propagation rays. Although this was not supported under the current study, it is of sufficiently similar interest that a description of the work has been included as Appendix A of this report.

5.0 GEOSAT ALTIMETER IN DATA FUSION

In recent years research has been conducted which shows that the GEOSAT altimeter data can be used in the analysis of the polar regions. As shown in Figure 1 altimeter data has been used to produce a number of different geophysical parameters. It is because of this that the altimeter data was explored for its possible additive contributions to data fusion. Because of the late start of this analysis in the program, we have only to date used the altimeter data as a comparison to SAR data. Figure 16 shows simultaneous plots of the altimeter ice index with SAR relative radar cross section values which have been manually divided into ice type. The SAR values came from a MIZEX '87 GEOSAT underflight collection just north of Iceland and is shown in Figure 17; the altimeter track was between the two white lines. Note the almost one-to-one correspondence between ice index peaks and SAR radar cross section peaks from the smoother multiyear areas. Manual analysis of the SAR data was performed to determine the type of ice that these peaks in the SAR intensity represented. It was determined that they were smoother multiyear ice whereas the lower SAR returns represented rougher first year ice; this analysis determined the ice type markings shown on Figure 16. This was consistent with other research (Fetterer, 1991) which indicated that the altimeter ice index would be lower for the rougher ice types.

An additional comparison was performed using SAR data collected over the Bering Sea during the Alaska collection. The GEOSAT altimeter collected simultaneous data over a small corner of the SAR data during this collection which allowed comparison of the altimeter ice index with SAR ice concentrations. Figure 18 shows a plots of the altimeter ice index along with SAR ice concentrations. The ice concentration estimates were derived manually from the optically processed digital SAR data. An ice concentration estimate was calculated for each of the altimeter

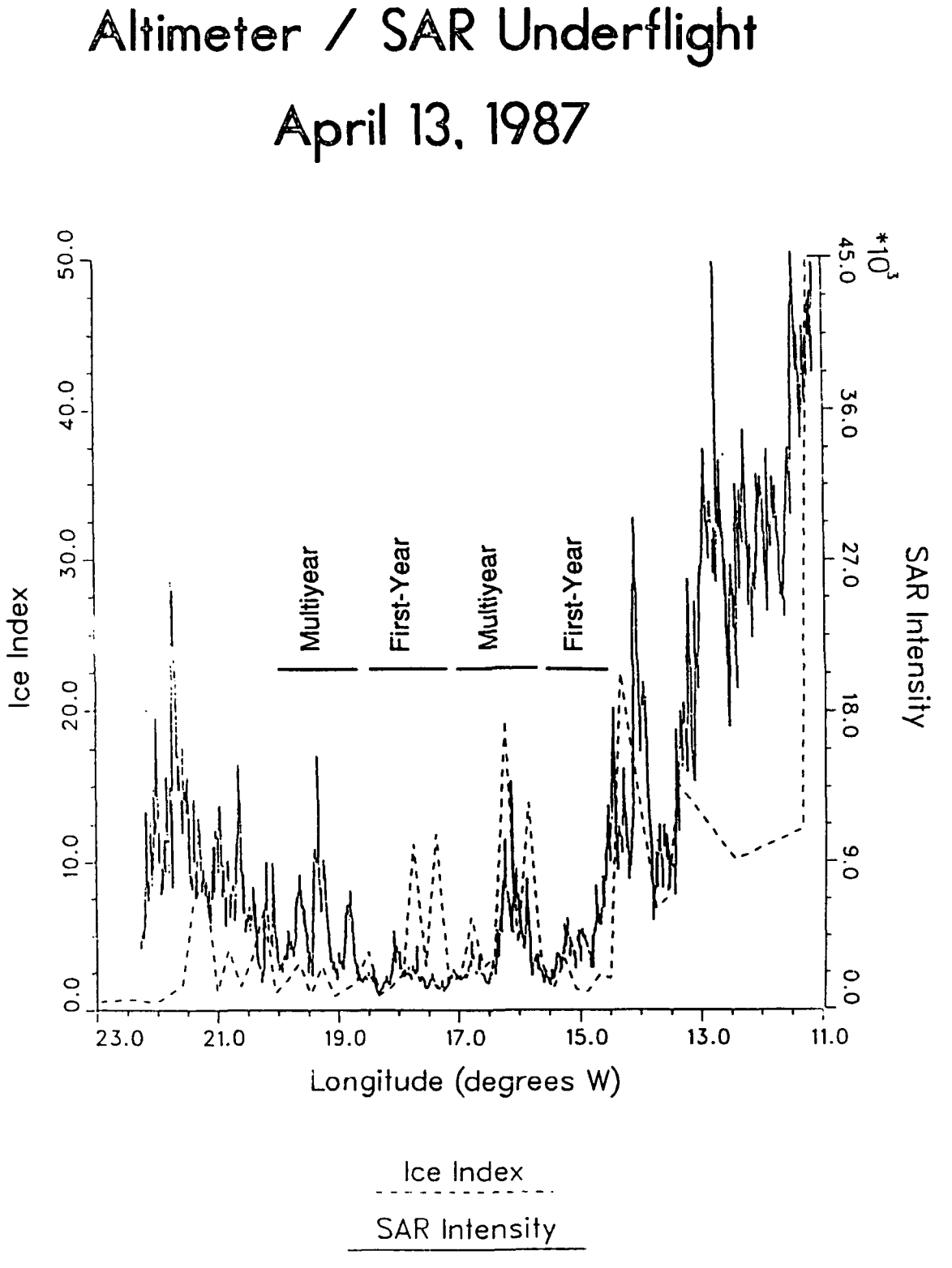

Figure 16. Altimeter/SAR Underflight, Comparison of Altimeter Derived Ice Index and SAR Intensity for 13 April 1987

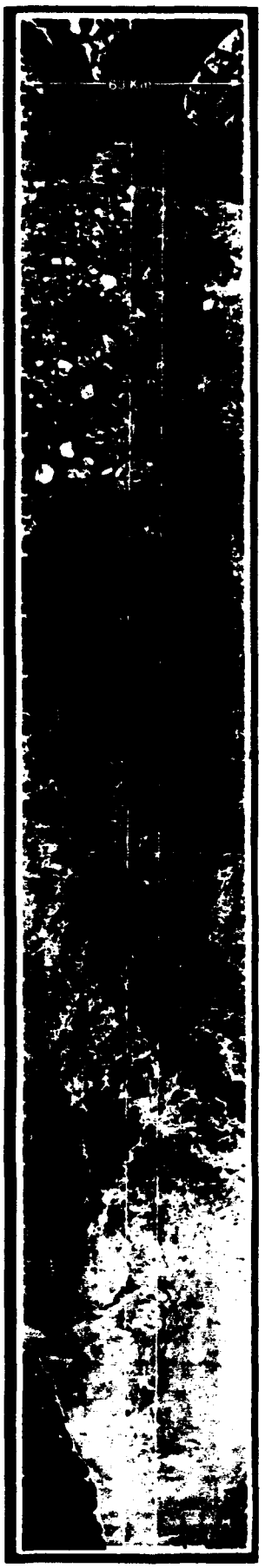

Figure 17. Altimeter / SAR Underflight, Optically Processed Image of SAR Data Collected During MIZEX '87, 13 April 1987, with Altimeter Path Denoted with White Lines

Altimeter/SAR Comparison

March 21, 1988

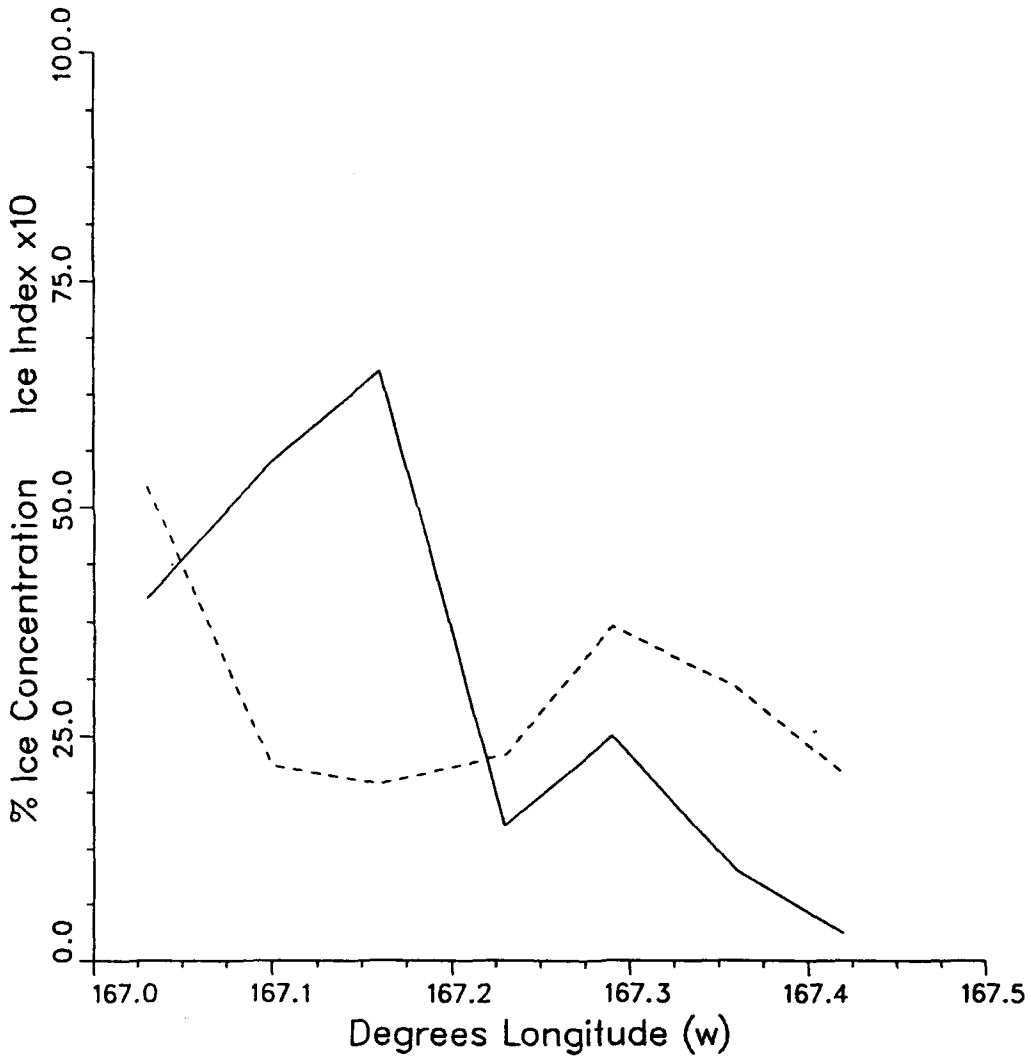

Figure 18. Comparison of SAR Derived Ice Concentration with Altimeter Derived Ice Index for 21 March 1988

footprints available in the SAR scene. It has been shown by Fetterer et al. (1991) that the ice index will drop over the rough ice and open water and will increase over the smoother first year ice. This phenomena was also observed in this data set. As shown in Figure 18, the ice concentration level increased to 65% at about 167.15° West. The manual analysis indicated that the amount of rough ice also increased which gave a lower ice index that stayed low over areas of a combination of rough ice and open water (to 162.2° West). As the percentage of smooth ice increased, (at about 167.25° West), the ice index also increased and then dropped as it moved out into the open water. It is important to note in this analysis, however, that although the ice index did fluctuate, the values remained relatively stable in terms of the observed ice index values over the ice/water boundaries in other regions and compared to the data shown in Figure 16.

This initial analysis of incorporating the GEOSAT altimeter into a data fusion study has shown consistency with previous results and indicated a good agreement with ice type and ice edge location using the SAR. As discussed in Section 7, future work on incorporating altimeter data into other geophysical estimates (ridges, floes, etc.) should be pursued next.

6.0 BETTER GEOPHYSICAL ESTIMATES FROM SENSOR FUSION

Although using data fusion for algorithm verification and generating maps of simultaneous geophysical information is useful to the analyst, the real advantage in data fusion is in generating new or enhanced geophysical estimates that can not be calculated as accurately from any one sensor. This type of analysis often involves using the strengths of one sensor to overcome the weaknesses of another sensor. This form of data fusion can be performed in a number of different ways. One method is to combine the geophysical outputs from one sensor to enhance the geophysical outputs from another sensor. A second method is to use the raw data values for two different sensors to give enhanced data products or to derive new geophysical parameters that neither of the one sensors alone can predict.

The first method involves much less effort than the second since numerous algorithms already exist which derive geophysical output products from the various sensors (as described in Section 2). One example of this method is the use of SSM/I low resolution total ice concentration values to help interpret the high resolution SAR samples. The SSM/I performs well in distinguishing open water from new ice on its low resolution grid, while the SAR has difficulty making this differentiation since both can appear dark in the SAR image data. Figure 19 shows an optically processed SAR mosaic obtained during the CEAREX data collection. It is very difficult (even for the trained researcher) to accurately determine if the darker regions in the mosaic are open water or new first-year ice. If the SAR mosaic is mapped over the SSM/I concentration estimates however (as shown in Figure 20 where the SAR mosaic extent is indicated by the blue polygon), an estimation of location of the new ice and first-year ice can be more accurately accomplished using the SSM/I values. That is, if the SSM/I indicates 20% open water over a 25 km region, this can be compared to the manual interpretation to determine if, in fact, approximately 20% of the total region

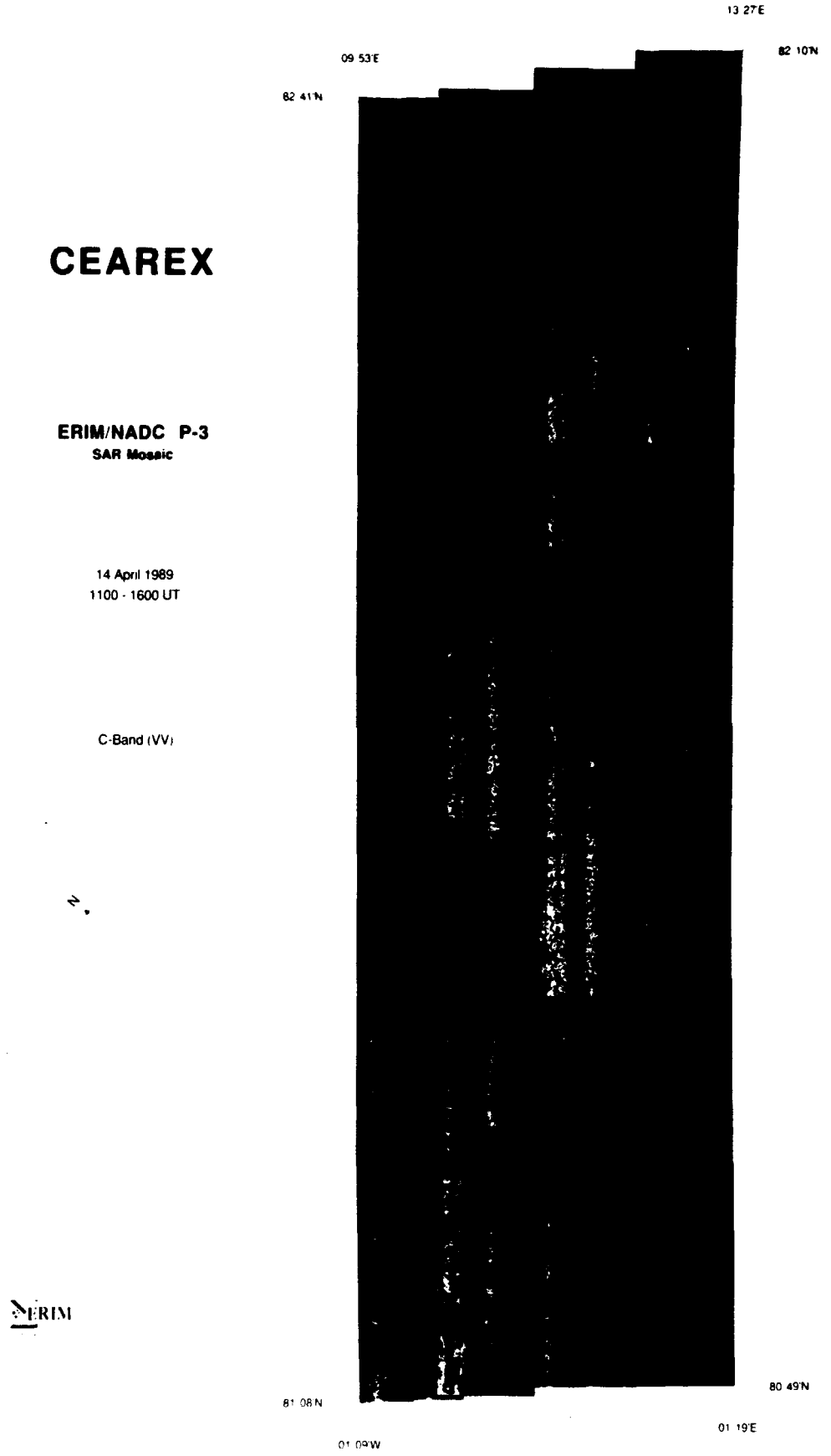

Figure 19. Optically Processed Mosaic of SAR Data Collected During CEAREX, 14 April 1989

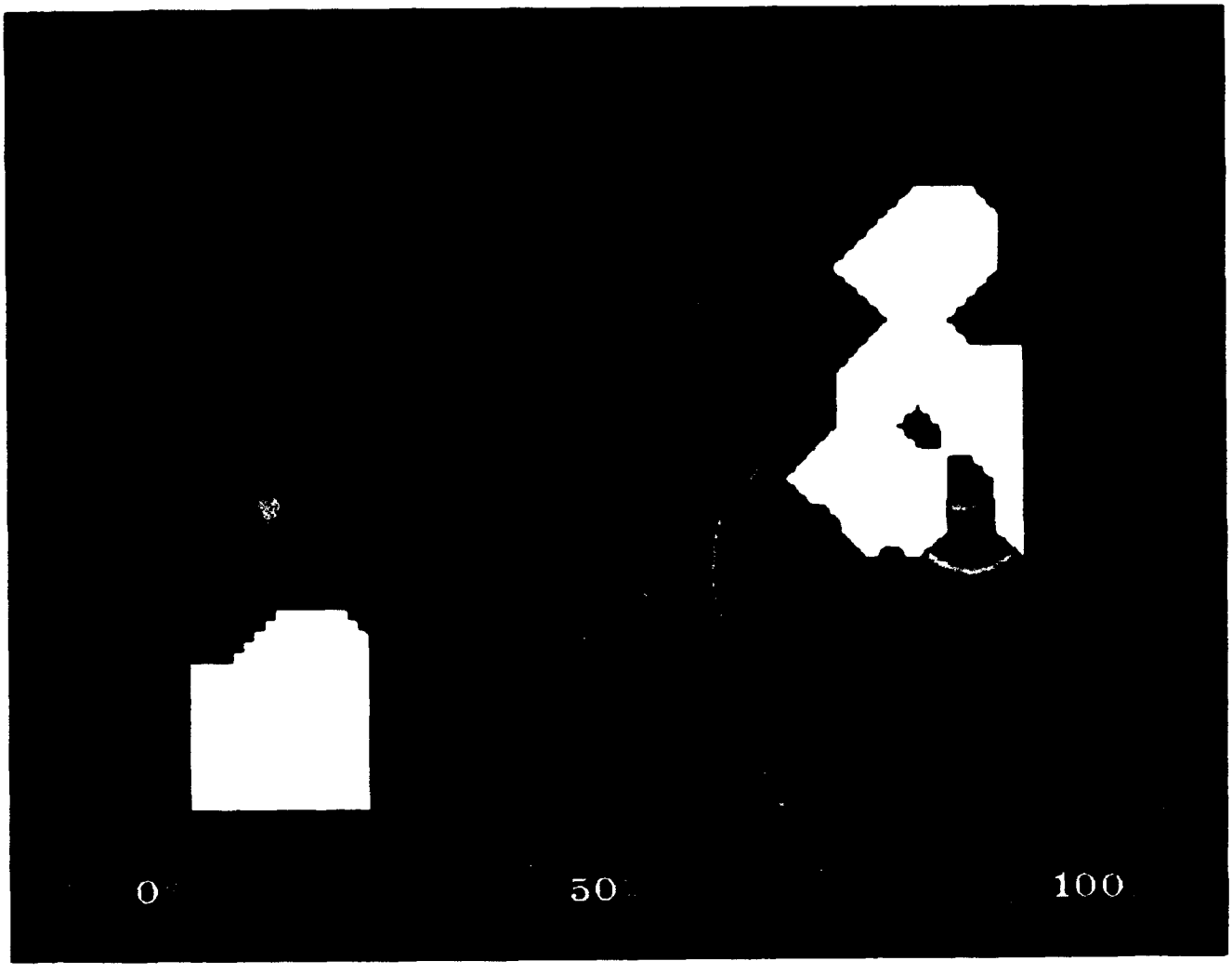

Figure 20. SSM/I Derived Total Ice Concentration During CEAREX, 14 April 1989, with SAR Mosaic Superimposed

was classified as open water. If not, then some of the darker SAR regions were misclassified. This estimation proved to be quite accurate when compared to the manual interpretation of the open water locations in the mosaic (see Figure 21); the SSM/I's estimation of ice concentration level drops to about 85% (giving 15% open water) over the areas where manual interpretation also detects about 15% open water.

The second method of data fusion described above is a much more difficult task, but its payoffs are far greater. This method ideally entails combining all of the raw sensor measurements into a global data set and deriving new algorithms for generating geophysical estimates that draw upon this global set. This is illustrated in Figure 22 where, in contrast to Figure 1, all of the sensor's raw measurements are put into a single geophysical estimation algorithm which then outputs the desired estimates. As indicated by the question mark, there is the potential for this approach to generate new estimates that individual sensors alone can not produce. This type of fusion would allow for the weaknesses of one sensor to be overcome by the strengths of another to produce new and more accurate geophysical estimates.

An initial effort of combining raw data products from two different sensors to generate more accurate geophysical products was performed on the 17 and 20 March CEAREX data sets. Areas of known ice types were extracted for the SAR, SSM/I and AVHRR data and the mean and variance for each ice type was calculated over all the subsets for each sensor. These results were then plotted for each pair of sensor measurements where the mean values were used as the center points and $\pm$ one standard deviation was used as the extent of the measurements in both directions. Figure 23 shows the results for comparing SAR intensity values with the individual SSM/I channels. The utility of these plots is as follows. The separation of the ice types in either the horizontal or vertical directions represents the ability of the individual sensors to differentiate between the ice types. If the separation of the ice types on the two dimensional cluster plots is greater than their separation either

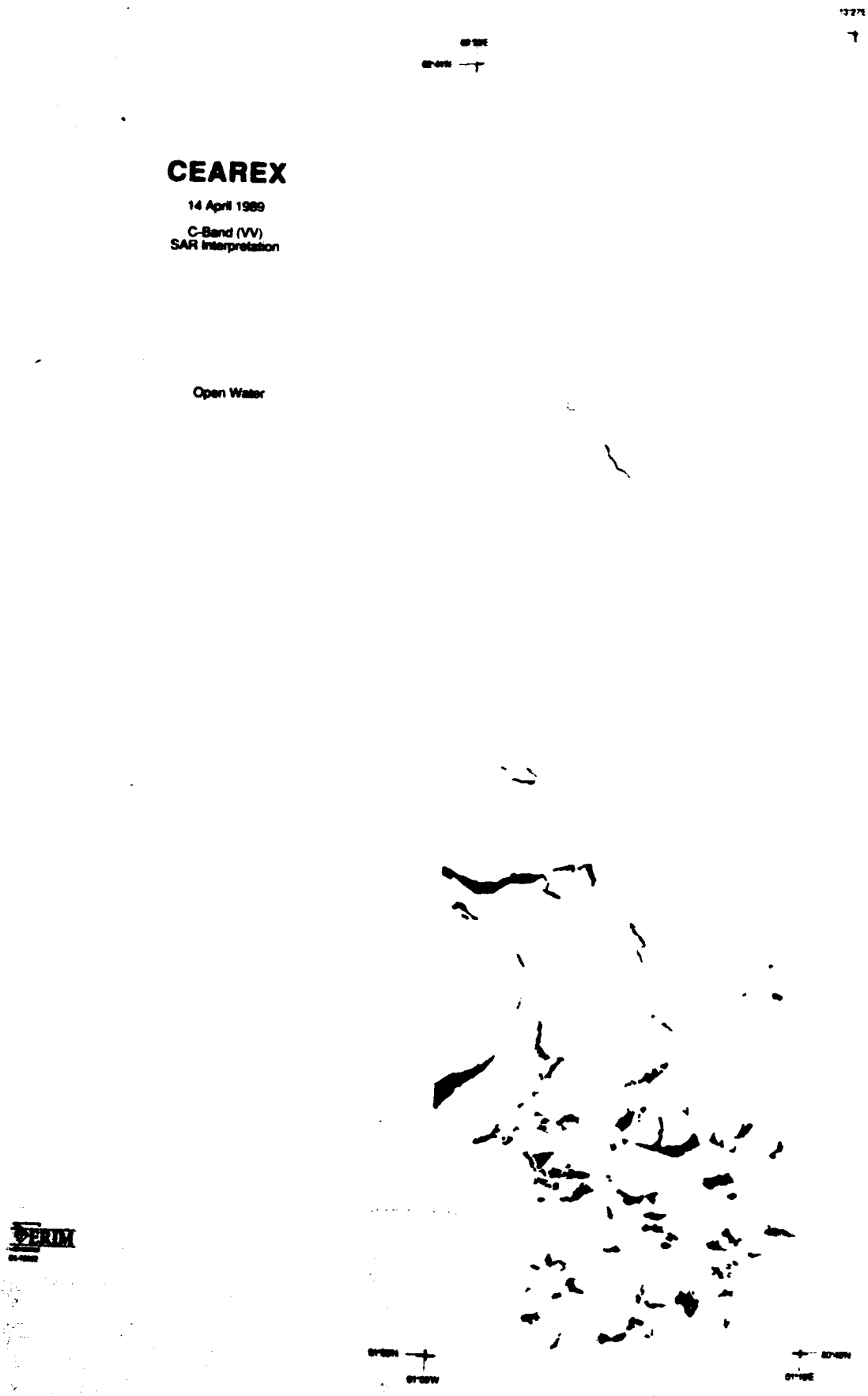

Figure 21. Manually Derived Open Water Locations from the 14 April 1989 SAR Mosaic

Geophysical Information Attainable from Sensors

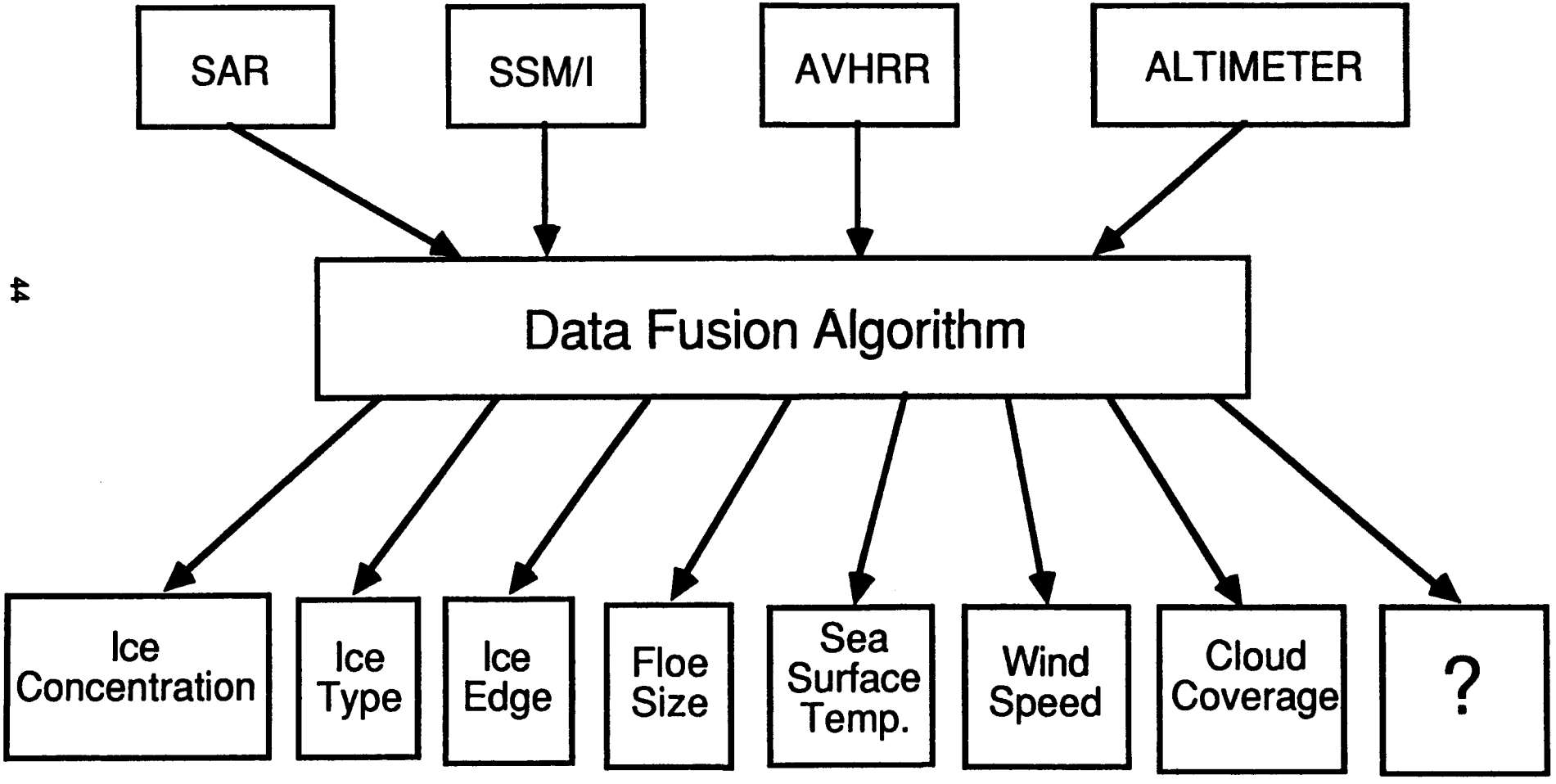

Figure 22. Summary of Geophysical Information Attainable by Combining Raw Sensor Data

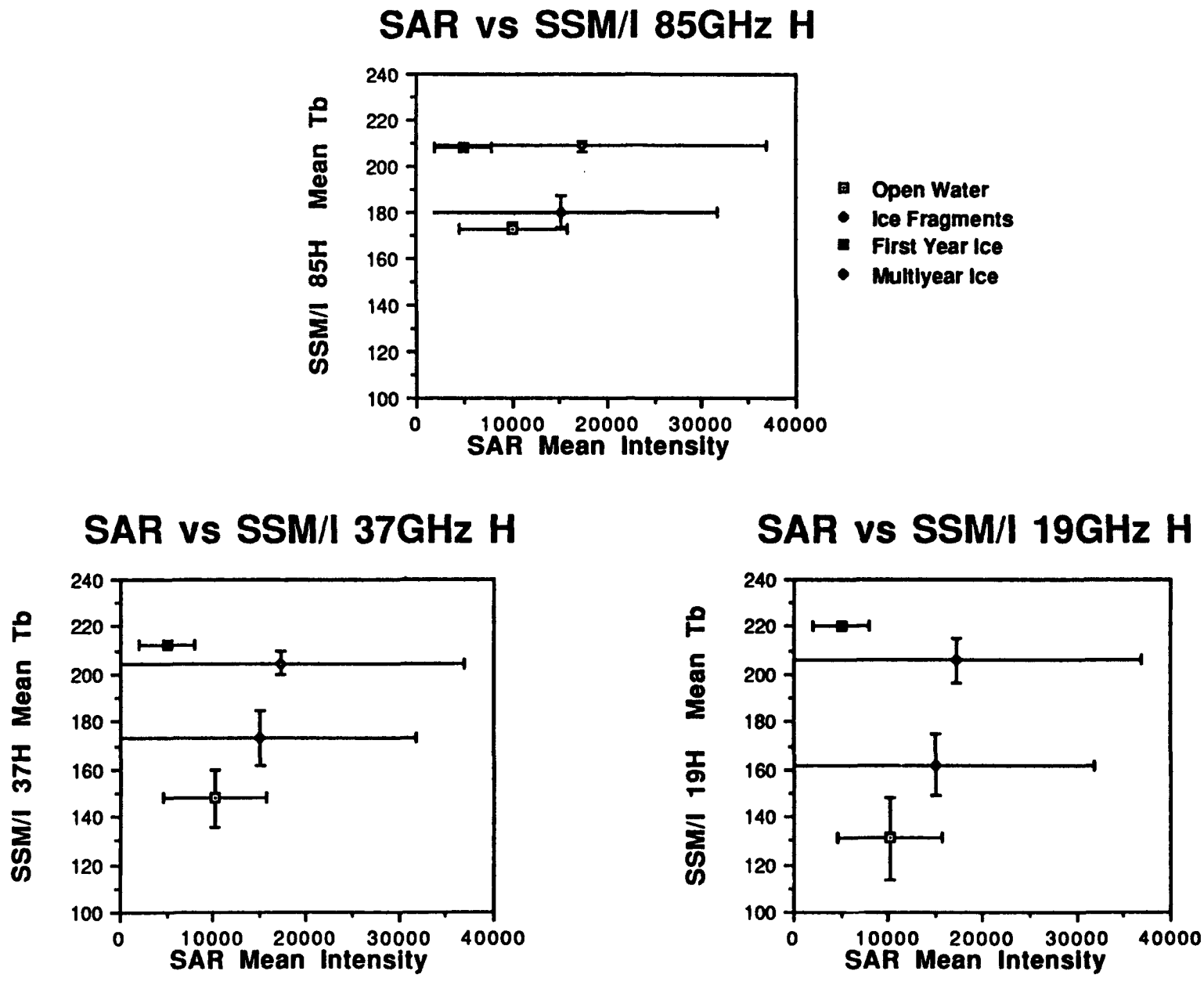

Figure 23. Fusion of SAR and SSM/I Raw Data Values Used to Separate Ice Classes, (a) SAR Intensity versus SSM/I 85 GHz Horizontal Channel, (b) SAR Intensity versus SSM/I 37 GHz Horizontal Channel, and (c) SAR Intensity versus SSM/I 19 GHz Horizontal Channel

vertically or horizontally, then the "fusing" of the two channels will generate better separation than any one sensor alone. Note that this represents the simplest combination of sensor data; i.e., taking them two at a time. Ideally, one would look at an N-dimensional plot combining all of the sensor measurements and determine if the resulting cluster separations was greater than for any single sensor. This is proposed in the follow-on effort.

It is clear in Figure 23 that each of the raw SSM/I values show separation between the ice type (especially between open water and first-year ice) whereas the SAR data indicates almost complete overlap. Thus, to generate high resolution ice type maps will require fusing both sensors; using the SAR to generate the high resolution and the SSM/I to provide the ice type classification. One approach would be to use the SSM/I values on its coarse sampling to guide the division of the SAR samples; i.e., if SSM/I shows 10% open water, then the lower 10% of the SAR samples are assigned to open water. Obviously, the utility of such approaches and their accuracy remain to be tested.

The potential of fusing the AVHRR data values with the SAR and SSM/I raw data values was also explored using this analysis. Figures 24 a) and b) show plots similar to the previous figure, but for SAR and AVHRR results. This analysis proved to be promising in differentiating first-year ice and open water using a combination of these two sensors. While these two data types could not be differentiated using either the SAR intensity values of the AVHRR channel 4 data values, a combination of the two shows a slight separation between clusters. This plot also shows a large separation between multiyear ice and each of the three remaining ice types when the SAR data is combined with the AVHRR channel 4 data.

Figure 24 c) and d) show plots for SSM/I and AVHRR. This shows slightly better differentiation between open water and ice fragments than the SAR with SSM/I since it slightly shifts the two classes vertically with respect to each other; thus

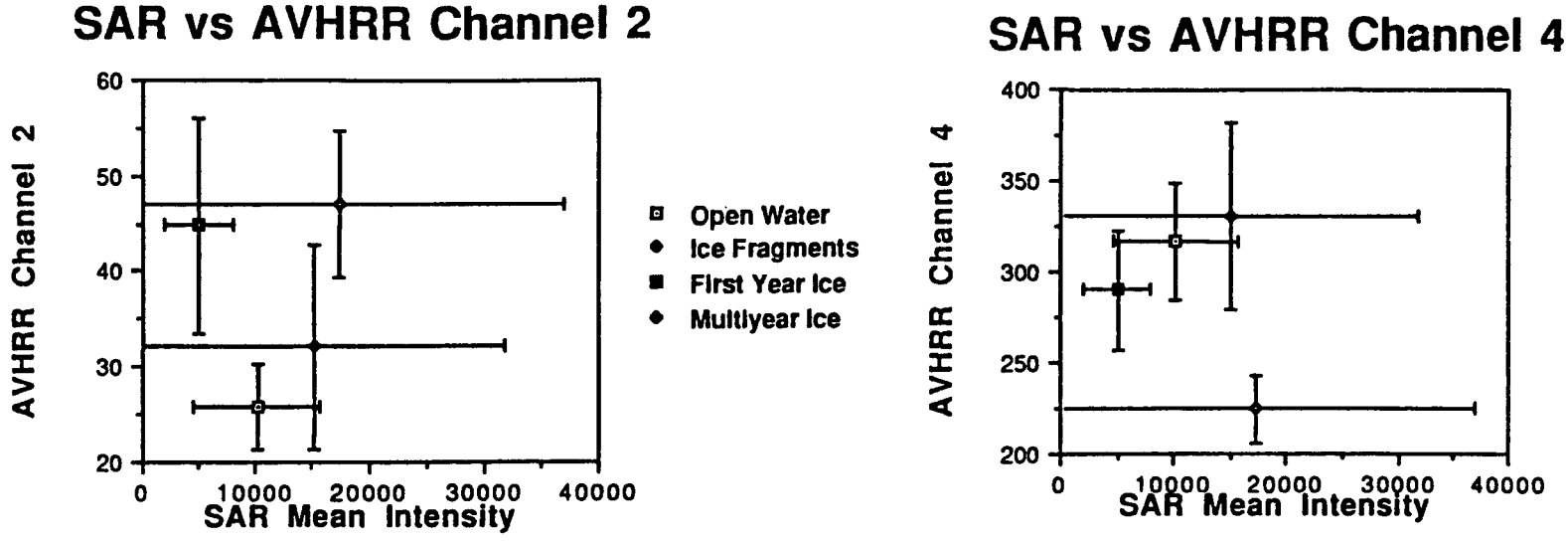

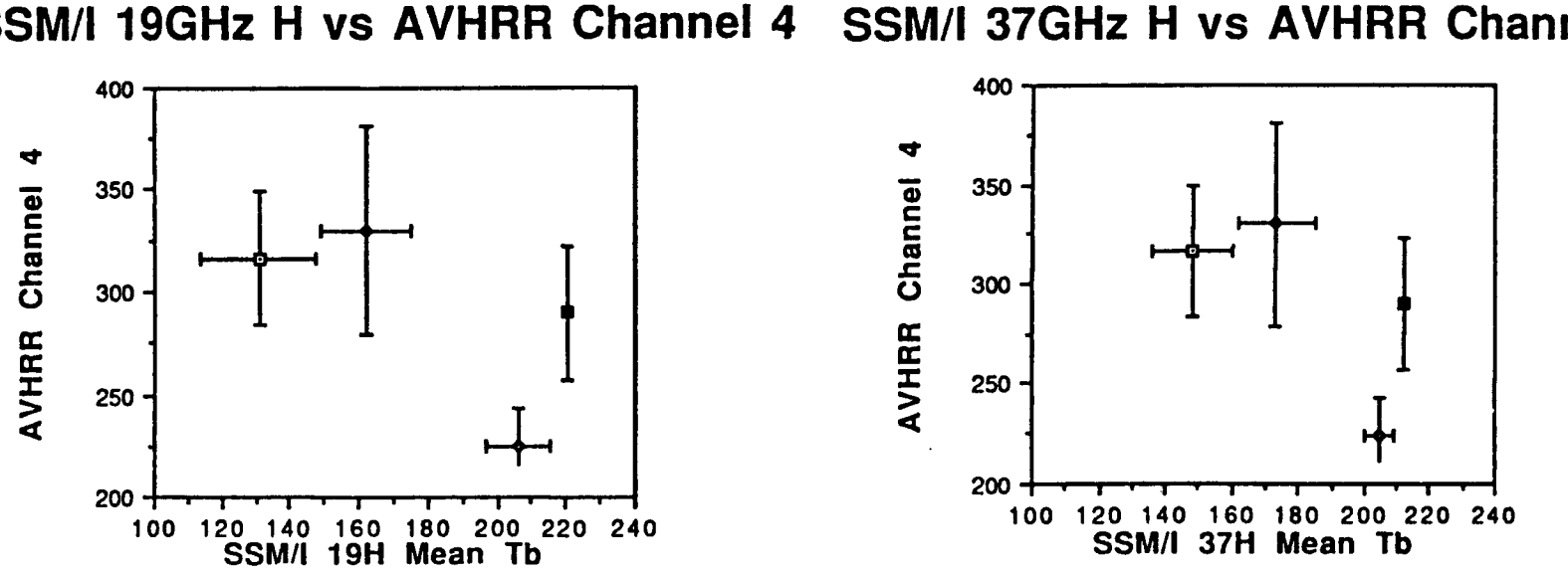

Figure 24. Fusion of AVHRR Data with SAR and SSM/I Raw Data values Used to Separate Ice Classes, (a) SAR Intensity versus AVHRR Channel 2, (b) SAR Intensity versus AVHRR Channel 4, (c) SSM/I 19 GHz Horizontal Channel versus AVHRR Channel 4 and (d) SSM/I 37 GHz Horizontal Channel versus AVHRR Channel 4

increasing the distance between them. Whether the usefulness of this is counteracted by the lack of AVHRR availability due to cloud cover remains to be tested, or whether the SSM/I can perform essentially as well alone.

Although these initial tests showed some potential in increasing ice classification using data fusion, this analysis (as well as future higher dimensional analysis) is limited to the ice types contained in the CEAREX data sets. To combat this limitation, either other data sets need to be incorporated, or more global results need to be interpolated from this data set. The former should be pursued, there is no model that is better than actual data, and we have proposed it as a follow-on task in Section 7, but we also started to address the latter approach by generating a more global SSM/I model. From previous studies we had generated SSM/I ice concentrations over the Bering and Beaufort Seas, and from the CEAREX data sets we generated SSM/I results over the Greenland Sea. This gave us a data set of SSM/I ice concentrations connected with SAR "truth" values; i.e., for each SSM/I concentration we had a ground truth value of total ice concentration and multiyear ice concentration. These values represent single samples of a more global SSM/I model that could predict the SSM/I concentration values for any ice concentration. That is, they represent single samples of the continuous functions T(t,m) and M(t,m) where t = actual total ice concentration within the SSM/I footprint, m = actual multiyear ice concentration within the SSM/I footprint, M = the SSM/I multiyear concentration estimate and T represents the SSM/I total ice concentration estimate. Generating such a model allows; (1) testing of algorithms on the SSM/I values for ice conditions not covered by a given experiment; and (2) checking of the consistency of SSM/I results over different arctic locations.

Figure 25 (a) shows the results of combining all of the SSM/I total ice concentration estimates for the three arctic locations and Figure 25 (c) shows the combinations of the SSM/I multiyear estimates. The actual ice type conditions are

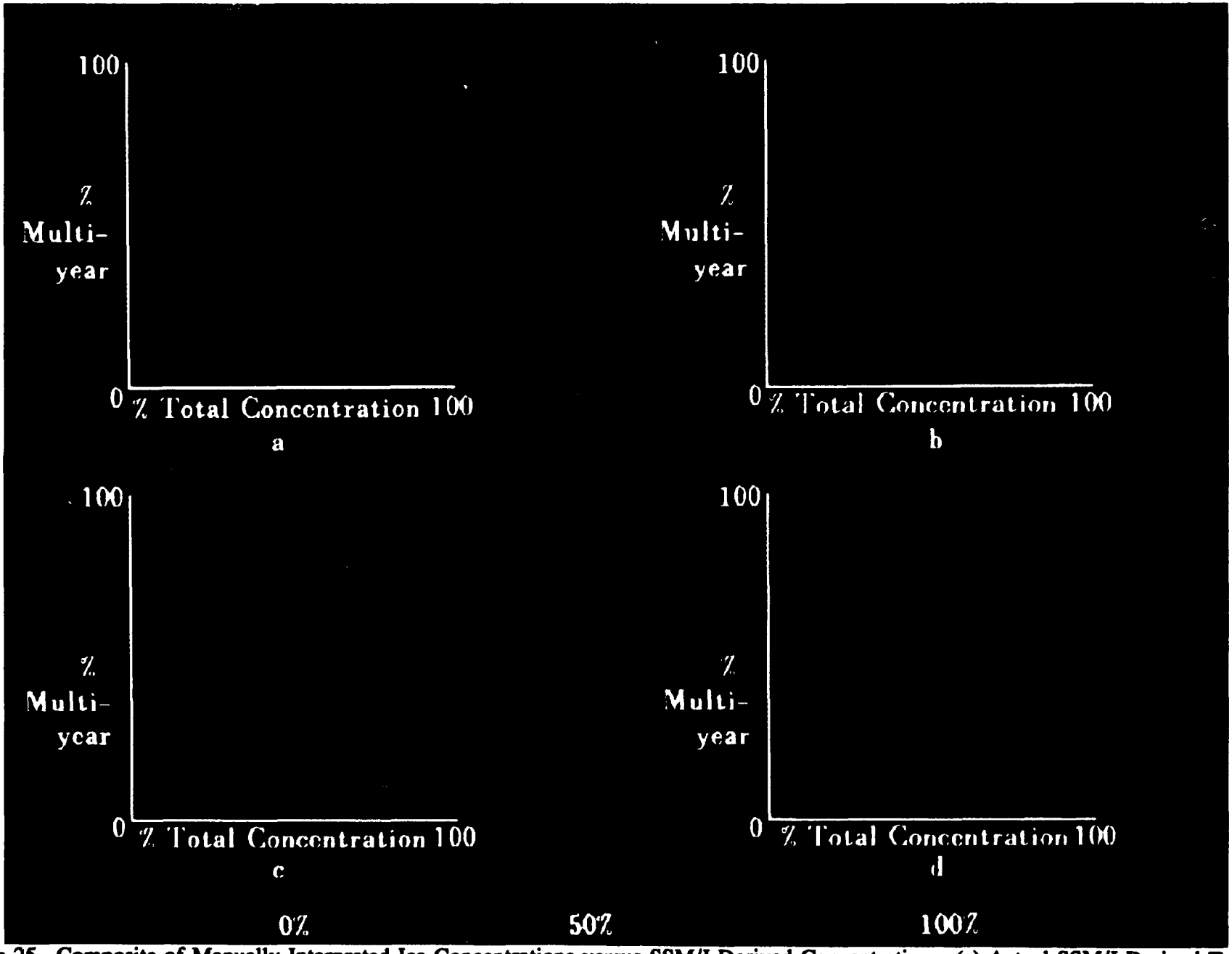

Figure 25. Composite of Manually Interpreted Ice Concentrations versus SSM/I Derived Concentrations, (a) Actual SSM/I Derived Total Ice Concentration versus Manually Derived Concentrations (b) 2-Dimensional Fit of SSM/I Derived Total Ice Concentration versus Manually Derived Concentrations, (c) Actual SSM/I Derived Multiyear Ice Concentration versus Manually Derived Concentrations (d) 2-Dimensional Fit of SSM/I Derived Multivear Ice Concentration versus Manually Derived Concentrations

plotted on the horizontal and vertical axis while the SSM/I values are shown as colored dots. The location of the dot represents the actual ice conditions in the SSM/I footprint while the color of the dot represents the SSM/I estimate value. The color bar on the bottom of the Figure translates the colors into concentration values. Figures 25 (b) and (d) show a spline fit to the data values and represent the first stage of generating this global model. A number of points should be noted. The model values will only exist below a 45 degree line since this represents the only possible values. A lack of data samples in the middle, bottom portion of the multiyear (bottom) plot generates the dark hole shown in the spline fit. If the SSM/I estimates were perfect, the model would show a plane going from left to right in the total concentration (top) plot and a plane going from bottom to top in the multiyear concentration (bottom) plot. Note that the total ice plot shows this in that it goes from very low (purple) colors to very high (red) colors from left to right almost linearly. This is consistent with the previous observation that the total ice concentration algorithm worked well. The multiyear algorithm on the other hand does not show good behavior indicating an underprediction of the multiyear values; again consistent with previous observations. Finally, note that these results do appear consistent among the different arctic locations. Except for the green dots at the very right of the multiyear (bottom) plot, all of the measurements appear smoothly varying between each other. The model fits also show this in that no abrupt oscillations are shown.

This represents the first step in performing more global data fusion tests. After generating similar models for AVHRR and SAR data, a statistical analysis of the different models could predict under what ice conditions data fusion would be most useful, and how well it could separate different ice conditions. This is discussed in Section 7.

In summary, the results from this form of data fusion are very encouraging. Combining pairs of raw sensor measurements indicated that an increase in separation of certain types of ice could be achieved that would be better than any single sensor. In addition, a start has been made to generating global models for predicting the responses on sensors to different ice conditions. The generated SSM/I model showed consistency between arctic regions and consistency with previous observations.

7.0 CONCLUSIONS AND FUTURE WORK

This study represents an initial step toward answering the fundamental data fusion question; can combining the raw data from different sensors provide additional geophysical products that individual sensors alone can not provide. This is a difficult question and additional work needs to be done to accurately answer it. In this study we have laid the foundation for that answer by: (1) Generating the registered data sets needed to test the fusion algorithms; (2) Developing the algorithms necessary to combine different sensor output products into a composite, spatial, map; (3) Demonstrating the increased potential of data fusion to separate specific ice types; and (4) Initiating the development of global SSM/I, AVHRR and SAR models to predict their raw data measurements over any type of ice conditions. Using these results, we can build the next stage of data fusion analysis and begin to develop specific algorithms for estimating geophysical products from the combined data sets. Specifically, our recommendations for future work are as follows.

One of the initially most promising data fusion algorithms is to combine the open water/new ice differentiation capability of SSM/I with the high resolution capability of the SAR. An indication of this potential was shown in this report where the SSM/I ice concentration results were used to establish that the darker regions in the SAR mosaic were open water and thus validated the manual interpretations. The automation of such an algorithm will be pursued, and although we can not anticipate the actual final form, we believe it will utilize the low resolution SSM/I estimate to chose which of the high resolution SAR samples are open water. For example, if the SSM/I predicts 10% open water, than the lowest 10% of the SAR pixels could be labeled as open water. Whether this is the optimum scheme, and how well it works, needs to be determined.

The global SSM/I model developed under this report has great potential for answering data fusion questions. It should be extended to the raw SSM/I data measurements (i.e., the individual channel values instead of the geophysical output products) and the models for other sensors generated. From these, a statistical analysis of the separability of the sensor measurements for different ice conditions could predict when data fusion could provide additional information and when it would only be redundant. An analysis similar to the cluster plots discussed in this report could also be performed for different ice types (i.e., dominantly first-year, dominantly multiyear, etc.) where, instead of just two sensor measurements, all of the sensor measurements would be included and the optimal combination of them for ice type separation calculated. A comparison of the resulting separations with the ability of each individual sensor to perform the same separation would determine the utility of data fusion.

This same analysis should also be applied to the CEAREX data sets for the specific ice types that it contains. A comparison of these results with the model results discussed above would give confidence to the model results and allow the more global application of the algorithms.

The potential of data fusion may also lie in other geophysical outputs instead of ice type classification, and these should be pursued. Using the manually interpreted SAR outputs that were generated in this study along with the registered CEAREX data sets, a comparison of SSM/I, AVHRR and GEOSAT altimeter measurements versus ridge and floe characteristics should be performed to determine if a correlation can be found. From this an algorithm for extracting the ridge or floe estimates from the combined sensors could be developed. This would be potentially the first automated algorithm for efficiently extracting these estimates and thus, very useful.

Finally, additional data sets of registered data from multiple sensors should be generated. Testing these results strictly on the CEAREX and MIZEX data sets could

be dangerous since they may not represent the full range of responses expected throughout the arctic region. One candidate is the data set reported by (Comiso, 1991) which contains SAR, passive microwave, upward and sidescan sonars, lidar profilometer, and infrared data. This data set contains much more actual ground truth measurements in terms of estimating the properties of the ice, and could be invaluable as a testing ground for the data fusion algorithms. In addition, data sets will soon be available that contain the ERS-1 SAR, ERS-1 altimeter, SSM/I and AVHRR sensors which will be invaluable in determining what strictly satellite based systems will provide. A possible upcoming mission that could provide this data is the LEADEX collection.

8.0 REFERENCES

Cavalieri, D.J., et al., "Aircraft Active and Passive Microwave Validation of Sea Ice Concentration from the DMSP SSM/I", JGR Oceans.

Comiso, J.C., et al., "Top/Bottom Multisensory Remote Sensing of Arctic Sea Ice", Journal of Geophys. Research, Vol. 96, No. C2, pp 2693-2709, February 15, 1991.

Fetterer, F.M., et al., "A Comparison of Geosat Altimeter and Synthetic Aperture Radar Measurements Over East Greenland Pack Ice", Int. J. Remote Sensing, Vol. 12, No. 3, pp 569-583, 1991.

Jentz, R.R., et al., "NASA, Navy, and AES/York Sea Ice Concentration Comparison of SSM/I Algorithms with SAR Derived Values", Proc. Int. Geoscience and Remote Sensing Symposium (IGARSS) Espoo, Finland, pp. 1587-1591, June 1991.

Gloersen, P., et al., "Reduction of Weather Effects in the Calculation of Sea Ice, concentration from Microwave Radiance", J. Geophys. Res., Vol 91, pp 3913-3919, 1986.

Hollinger, J., "DMSP Special Sensor Microwave/Imager Calibration/Validation", DMSP Final Report Vo. 1, Space Sensing Branch of the Naval Research Laboratory, Washington, DC, July 1989.

APPENDIX A

ACOUSTIC TOMOGRAPHY SUPPORT

APPENDIX A: ACOUSTIC TOMOGRAPHY SUPPORT

An example of how the compilation of various sensors can be used to produce more detailed pictures of a study region was explored recently in Environmental Research Institute of Michigan's (ERIM's) sensor fusion support of the Acoustic Tomography Experiment funded under another contract. During this experiment, six moorings were deployed in the Greenland Sea in the Fall of 1988. Five of the moorings were placed in a pentagonal array with the sixth mooring in the center of the pentagon (see Figure A-1 and Table A-1). Data was collected on-board the moorings numerous times during a day for an entire year (September 1988 - August 1989).

ERIM's support of the Acoustic Tomography work included the development of weekly ice concentration, wind speed, and sea surface temperature maps over the mooring array on a five by five kilometer grid (see example in figure A-2). This data was generated from both the SSM/I and AVHRR data sets.

1. TOTAL AND MULTIYEAR CONCENTRATION ESTIMATES

Total and multiyear ice concentrations were obtained for the Acoustic Tomography support from SSM/I data on a weekly bases from September 1, 1988 - February 14, 1989 and again from April 1, 1989 - August 31, 1989. Ice concentration maps were generated on daily bases from February 15, 1989 - March 31, 1989. Due to a rapidly moving Odden Event that occurred over these days, it was necessary to produce concentration estimates on a daily bases.

Both the total and multiyear ice concentrations for September 1988 - March 1989 were derived on a 50 km grid using the NASA sea ice algorithms. The data for these algorithms were also obtained from the NSIDC CD-ROM data set. A subset of the ice concentrations were taken over the acoustic tomography mooring array based on their

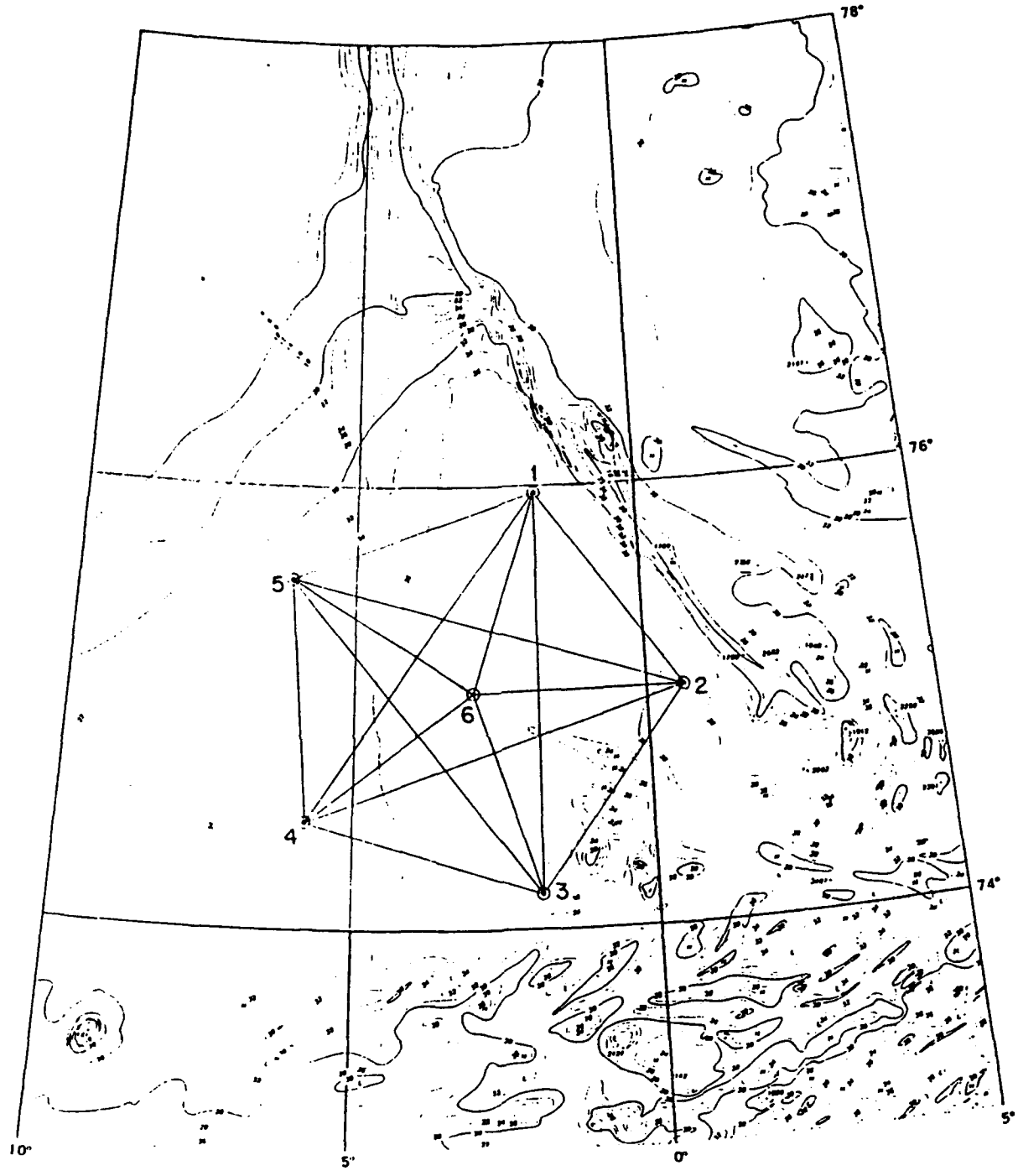

Figure A-1. Locations of Six Moorings Deployed for the Acoustic Tomography Experiment

Table A-1. Summary of Acoustic Tomography Moorings

Mooring	Position (Loran C)	Water Depth (Corrected m)	Anchor Deployment Year	Day	Time (UTC)	Anchor Release Year	Day	Time (UTC)	Electronics S/N	Source S/N
1	75°58.08'N, 001°50.00'W	3709	1988	260	1533	1989	233	1755	AVATAR 4	4
2*	75°03.69'N, 000°40.25'E	3717	1988	266	1331	1988	272	0900	AVATAR 2	2
3	74°09.38'N, 001°52.90'W	3735	1988	271	1341	1989	234	0959	AVATAR 3	3
4	74°28.90'N, 005°47.30'W	3466	1988	262	1320	1989	251	0425	WHOI 11	5
5	75°34.27'N, 006°07.70'W	3379	1988	258	1342	1989	242	2125	WHOI 12	6
6	75°03.60'N, 002°58.00'W	3629	1988	264	1407	1989	233	0333	AVATAR 1	1
7*	75°03.88'N, 000°38.20'E	3716	1988	273	1339	1989	232	0709	AVATAR 2	2

* Redeployment of Mooring 2.

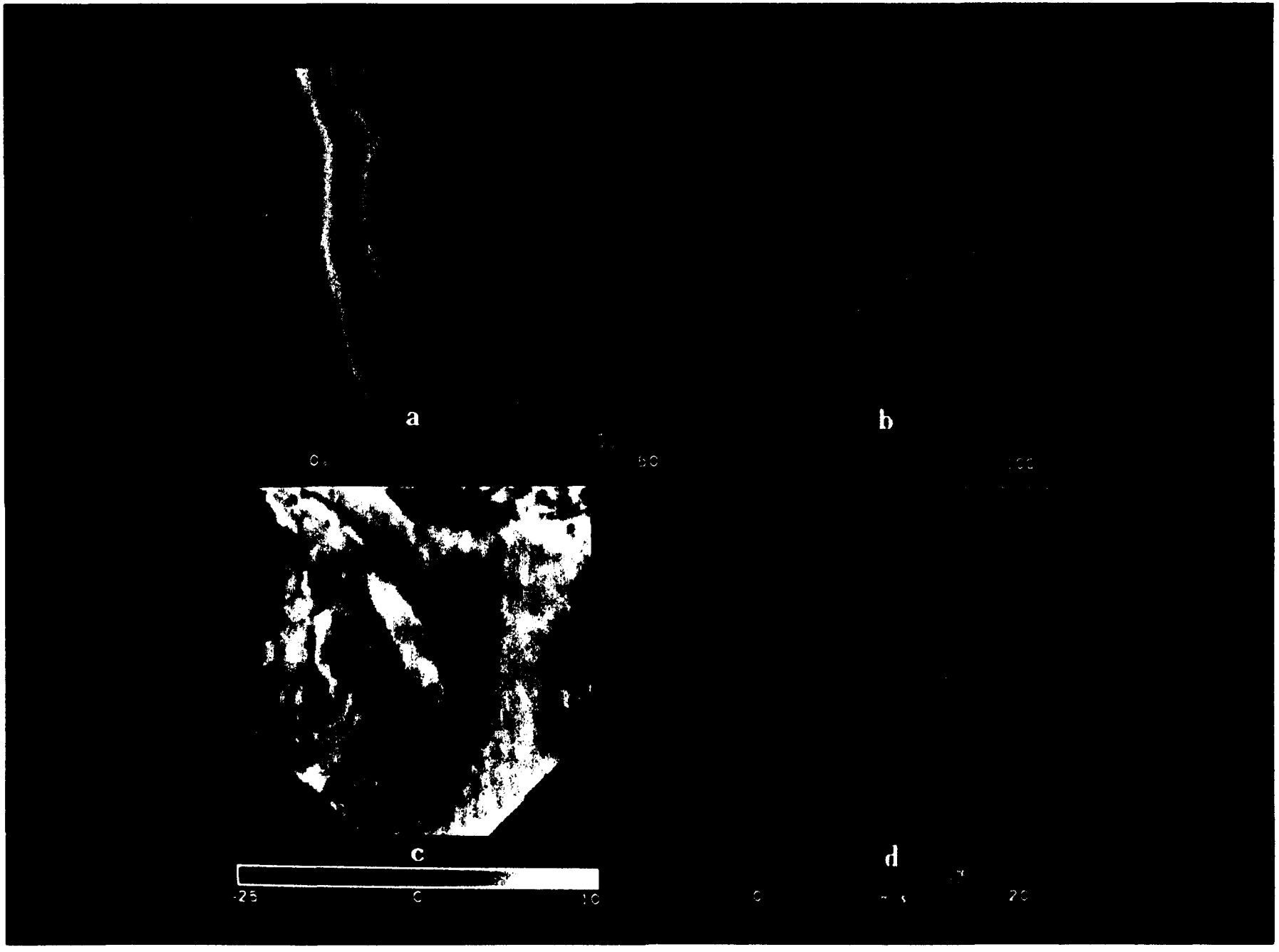

Figure A-2. Example of Data Fusion in Acoustic Tomography Support Work, 500 X 500 km Area on a 5 km Grid, (a) SSM/I Derived Total Ice Concentration, (b) SSM/I Derived Multiyear Ice Concentration, (c) AVHRR Derived Sea Surface Temperature and (d) SSM/I Derived Near Surface Wind Speed

latitudinal and longitudinal locations. The subset was a 500 X 500 km area covering from about 77° N to 73° S and from about 10° W to 6° E. This subset was then upsampled to a 5 km grid spacing using a bilinear interpolation scheme thus giving ice concentration maps of 100 records by 100 elements.

The total and multiyear ice concentrations for April 1, 1989 - August 31, 1989 were calculated from data generated by Ralph Gibson in the ERIM Washington DC Office. Mr. Gibson processed the SSM/I data with a NASA Goddard Space Flight Center computer account under approval of Per Gloersen at NASA. The algorithm that he used was written by Mr. Gloersen and his colleagues at NASA Goddard. This algorithm generated concentration maps on a 10 km grid. Both the total and multiyear concentrations were given in percentages (0-100%).

Like the concentration values that were obtained form CD-ROM, each pixel was mapped to a latitude and longitude location and then a 500 X 500 km subset was taken from the data. This data was upsampled from its 10 km grid to a 5 km grid using a bilinear interpolation scheme giving a 100 X 100 pixel output file.

Color hard copies of the total and multiyear ice concentration maps for all of the dates listed above were generated on the SUN workstation and copies were distributed to Jim Lynch (@WHOI), Peter Worcester (@Scripps), and Peter Wadhams (@SAIC). The data was also converted to ASCII format and sent to Jim Lynch and Arthur Newhall (@WHOI) for direct comparisons to the acoustic tomography data derived from the six moorings. The ice concentration data files and copies of the color images for all of the data are archived at ERIM in the Center for Earth Sciences.

2. NEAR SURFACE WIND SPEED ESTIMATES

Near surface wind speed was also derived from the SSM/I data on a weekly basis for most of the acoustic tomography year and on a daily basis during the Odden event (February 15, 1989 - March 31, 1989). The CD-ROM data was used again to

calculate the wind speeds for September 1988 through March 1989. Mr. Gibson at ERIM's Washington Office generated the data for April 1989 through August 1989.

The processing of the near surface wind speed with the SSM/I data from CD-ROM was very similar to the processing of the ice concentrations from CD-ROM. The Navy SSM/I wind speed algorithm was used to process this data. This algorithm uses the 25 km gridded brightness temperatures and therefore produces images on a 25 km grid. Similar to the concentration algorithm, a 500 X 500 km area was subsetted over the acoustic tomography mooring array and the data was upsampled to a 5 km grid. This area corresponded directly with the subset generated for the ice concentration results.

The data generated at our Washington Office was again generated on 10 km grid and upsampled to a 5 km grid over the acoustic tomography moorings. The subset taken was the same subset which was taken from the CD-ROM wind speed data. As with the ice concentration data, hard copies of this data and corresponding ASCII data files were generated and sent to the same people listed above.

3. SEA SURFACE TEMPERATURE ESTIMATES

Sea surface temperature was derived from AVHRR data. This data was taken from channel 4 (infrarred channel) of the AVHRR Local Area Coverage (LAC) data from the Greenland Sea area. This data was given to Jeff Hawkins at NOARL for image registration. Registration was done by using the ephimerous data and the visible AVHRR channel (to verify locations of land masses).

Both channel 2 and channel 4 data was sent to us from NOARL for the following 33 dates during the acoustic tomography year: September 11, 26, 1988; October 10, 1988; November 20, 27, 1988; December 17, 1988; February 11, 17, 20, 27, 1989; March 8, 17, 20, 21, 1989; April 1, 9, 17, 1989; May 2, 9, 17, 26, 31, 1989; June 5, 11, 21, 28, 1989; July 3, 13, 18, 29, 1989 and August 9, 20, 29, 1989. These

dates were chosen based on the availability of the AVHRR data in this region. The brightness temperatures available from the channel 4 data were converted to sea surface temperature in degrees celsius.

In order to compare this data with the SSM/I data products the resolution of the images were degraded to 5 km by performing a five by five contracting smooth on each of the images. Once the images were contracted, a 500 x 500 km subset (corresponding to the subset taken for the SSM/I data products) were taken from each image. As with the ice concentrations and near surface wind speed data, hard color copies of the images were generated and the data was converted to ASCII and sent to each of the researchers listed above.

4. ACOUSTIC TOMOGRAPHY VIDEO

A video was produced of all of the SSM/I data products that were generated for the acoustic tomography support work. The video was produced on the SUN workstation and was filmed with a video camera off the computer screen. The video consisted of a total of six segments. The first three segments were of the acoustic tomography subset described above sampled twice a month from September 1988 through August 1989. The last three segments were of the same subset sampled daily from February 15, 1989 through March 31, 1989 (the Odden event).

Each of the six segments were filmed at three different speeds. First, three cycles of the event are shown fast so as to get an overview of the entire time frame. Next, the video is slowed down and three more cycles of the event are shown so as to get a more detailed understanding of what is happening as time progresses. Finally, the video is sped up slightly again and two more cycles are shown so as to get a final look at the entire time frame.

The six segments progress in the following order:

Segment 1: Total Ice Concentration	9/1/88 - 8/31/89
Segment 2: Multiyear Ice Concentration	9/1/88 - 8/31/89
Segment 3: Near Surface Wind Speed	9/1/88 - 8/31/89
Segment 4: Total Ice Concentration	2/15/89 - 3/31/89
Segment 5: Multiyear Ice Concentration	2/15/89 - 3/31/89
Segment 6: Near Surface Wind Speed	2/15/89 - 3/31/89